ISSN: 2754-6675

Journal of Chemistry & its Applications

SCIENTIFIC Research and Community

Review Article

Open Access

Calculating Electron and Proton Properties Using the Ulianov String Theory

Policarpo Yoshin Ulianov

R&D Department, Power Opticks Tecnologia, Av Luiz Boiteux Piazza, Florianópolis, 88056-000, SC, Brazil

ABSTRACT

Ulianov String Theory (UST) introduces a geometric and dynamical reinterpretation of the fundamental constituents of matter by treating electrons and protons not as point-like particles but as extended spherical membranes formed by the collapse of imaginary time in a five-dimensional wormhole-based framework. Each particle is modeled as an Ulianov String, a chain of N_S Planck-scale wormhole copies that folds into stable three-dimensional configurations capable of reproducing known atomic properties while revealing new internal structures that organize protons and neutrons in the atomic nucleus and electrons in the electrosphere.

At the proton scale, UST predicts a structured spherical membrane arranged in onion-like layers, with electric charge distributed over all membranes and mass concentrated at a small point located at the pole of each layer, so that the proton mass may be viewed as a small cylinder. Alternatively, the proton can behave as a hemispherical shell of negative charges with the mass positioned along a circular ring, a configuration that arises when the spherical membrane is cut in half. These features naturally account for the observed variation of the proton radius, its magnetic moment, and the emergence of Strong Gravitational Contact Forces (SGCF), which provide a clearer explanation than the conventional strong nuclear force for the formation and stability of atomic nuclei.

For electrons, UST proposes a rotating spherical shell with Planck-length thickness and a large radius (from micrometers down to 5 nanometers depending on context), with charge spread across the membrane and mass concentrated asymmetrically at a polar point. This geometry simultaneously explains quantum-wave behavior, spin orientation, orbital formation, and electron–electron interactions. Applying these structures to atomic hydrogen, we compute electron and proton geometries that match the Bohr radii, Rydberg energies, and ground-state stability with high precision. The same membrane kinematics predicts elastic electron–proton interactions, UWH clustering, shrinkage of the electron radius, and expansion of the proton radii inside atoms.

We also derive the electrodynamic consequences of the UST particle geometry, showing how the extended electron shell naturally leads to Ulianov's reformulation of Maxwell's equations, in which the current density emerges from polarization and magnetization fields generated by shell dynamics. This provides a unified microscopic foundation for classical electrodynamics, superconductivity mechanisms, and electron transport in metals, insulators, liquids, and vacuum.

Overall, this work shows that the UST membrane model of electrons and protons yields quantitatively accurate atomic predictions, including a method for computing the radius and mass of these particles, which no theory in modern physics has achieved. Furthermore, UST clarifies the physical meaning of the fine-structure constant α (with 1/α=137), relating it to the existence of 137 layers in the electron membrane, which reduces the effective electron charge (to 1/11.7 of its maximum theoretical value in UST) and causes the gravitational force between two Planck-mass bodies to be 137 times weaker than the electric force between two electrons at the same distance.

The electron and proton configurations in UST reveal deeper geometric patterns from which nucleon behavior emerges naturally. The proton-neutron structures follow from the SGCF, and each proton configuration (hemisphere or sphere) determines the associated electron configuration (cap or spherical shell), providing a new way to understand and organize electrons in the electrosphere, in an analogy with Russian nesting dolls.

Although this framework differs significantly from how modern physics interprets protons, electrons, neutrons, and the atomic structures they form, the UST model elucidates several longstanding physical mysteries and computes quantities that no current atomic model can reproduce. Even if the theory is not entirely correct, the convergence of so many independent results makes it unlikely that these findings arise by coincidence. Thus, UST almost certainly captures aspects of atomic reality that remain inaccessible to current theoretical models. At the very least, it can serve as a powerful source of inspiration and new ideas for rethinking modern physics and for addressing several open problems that remain major challenges in the field.

***Corresponding author**

Policarpo Yoshin Ulianov, R&D Department, Power Opticks Tecnologia, Av Luiz Boiteux Piazza, Florianópolis, 88056-000, SC, Brazil.

Received: December 08, 2025; **Accepted:** December 17, 2025; **Published:** December 24, 2025

Introduction

Since the early twentieth century, physicists have sought a coherent understanding of the composition and nature of electrons, protons, neutrons, and the atomic structures built from them. The Standard Model of particle physics successfully predicts many observable properties—mass, charge, magnetic moment, scattering cross sections—yet these values ultimately depend on deeper assumptions about quarks, gluons, and other mediating particles. In practice, this framework transfers the explanatory burden from one level to another: instead of explaining why the proton has a given mass, it explains the mass of the proton in terms of the masses of more fundamental constituents, which themselves require explanation.

Moreover, the Standard Model treats electrons as point-like objects without spatial structure. While this description works remarkably well at atomic scales, it leaves several conceptual questions unresolved:

- Why does the electron exhibit both wave-like extension and particle-like localization?
- Why do electromagnetic interactions emerge with such precision from apparently structureless point charges?
- What is the physical meaning of the fine-structure constant α?
- Why is gravity enormously weaker than electromagnetism, although the gravitational force between two Planck masses at the same distance is 137 times larger than the electric force between two electrons? So why, for the same distance, if each particle has the maximal theoretical individual mass and the maximal theoretical individual electric charge, is the gravitational force larger than the electric force?
- Why does Pauli's exclusion principle work, given that electrons repel each other strongly and no known force binds electrons inside atomic orbitals?
- Why do two hydrogen atoms form a covalent bond despite the strong Coulomb repulsion between their electrons?
- Why does helium not form stable chemical bonds, and why do exactly six other atoms join it as noble gases?
- Why do metals form extremely strong crystalline structures described as "electron clouds," even though point-electron clouds offer no binding mechanism?
- Why do atomic electrons possess "two spins," while free electrons in vacuum or metals generate magnetic fields with a spin orientation always determined by the left-hand rule?
- Why is it that of Maxwell's four highly symmetric equations, only one (Ampère–Maxwell) contains an additive term?
- Why does the proton appear as a composite object whose measured radius varies depending on the probing method, and so does the proton radius appear to change in muonic-hydrogen experiments?
- Why are photon and electron wave functions given in values of probability collapse and produce real charge densities and real intensity amplitudes?
- What is the true microscopic meaning of the wave-particle duality observed in photons, electrons, and in principle in all particles?

Ulianov String Theory (UST) offers a unified and innovative set of answers to these questions by proposing a radically different microscopic ontology. Instead of point particles or uniformly dense spheres, UST describes electrons, protons, neutrons, photons, and even quarks as extended membranes generated by the collapse of imaginary time in a five-dimensional framework. At the foundation of UST lies a single elementary object: the Ulianov Wormhole (UWH), a refined version of the Einstein–Rosen bridge capable of traversing walls of space and time.

In UST, every particle corresponds to a single UWH evolving in five-dimensional kinematics (x,y,z,t,q), where time is complex ($s=t+iq$) and the imaginary component q advances discretely. When q collapses, the UWH appears in real spacetime as an Ulianov String (US): a chain of N_S identical Planck-scale wormhole copies arranged in sequence. This string has a fixed physical length $N_S\, L_P$, which is the same for electrons, protons, neutrons, and photons. Depending on how this universal string folds, it forms a thin spherical shell (electron), a compact volumetric sphere (proton), or a cylindrical four-dimensional structure (photon). These are not metaphors but literal geometric membranes whose topology and dynamics determine observable masses, radii, moments, and interaction strengths.

The purpose of this article is to compute the fundamental properties of protons and electrons directly from UST geometry, without invoking empirical constants beyond those at the Planck scale. We show that proton mass, proton radius, electron mass, and the free-electron shell radius arise naturally from simple geometric relations involving the winding number $137=1/\alpha$, the number of overlapping membrane layers in the electron shell, and the folding constraints imposed by imaginary-time collapse.

Applying the model to hydrogen, we derive elastic interactions between the solid proton membrane and the spherical electron shell. These interactions reproduce Bohr radii, Rydberg energies, and molecular bond lengths with high accuracy. The dynamics of the membrane also explain how the electron shell shrinks and the radius of the proton sphere grows inside the atoms, expands to approximately 5 nm when free and contracts under relativistic acceleration in agreement with the de Broglie wavelengths.

Finally, we connect these membrane geometries to classical electrodynamics by showing how polarization and magnetization fields arise directly from the motion and deformation of the electron shell. This provides a microscopic geometric foundation for Maxwell's equations and yields a unified explanation for conduction, insulation, and superconductivity.

An important historical remark concerns the Einstein–Rosen bridges that inspired UST. Einstein and Rosen attempted to construct a unified theory based only on gravitational and electromagnetic fields. When asked how such a theory could work without nuclear forces, Einstein is said to have replied that nuclear forces would not be necessary in a correct formulation. Though dismissed at the time, this intuition aligns naturally with UST: if proton and electron masses are concentrated in point-like poles that can come into direct contact at Planck-scale separations, then a Strong Gravitational Contact Force (SGCF) arises automatically. This SGCF reproduces all essential features attributed to the strong nuclear force and simultaneously explains electron–electron binding in orbitals and molecular formation, solving three parallel problems with a single physical mechanism.

If SGCF is real, then the standard nuclear forces may not exist as fundamental interactions. The consequences of this possibility are profound: it would open the path to a genuine theory of everything based on Einstein's late ideas and avoid the conceptual tensions of trying to unify real physical phenomena with forces invented purely for lack of microscopic knowledge.

The remainder of the paper is organized as follows. Section 2 reviews the historical development of atomic models and the motivations for a geometric reinterpretation of the electron structure. Section 3 presents the foundations of UST. Sections 4

and 5 derive the electron and proton geometries. Sections 6–12 present the full UST calculations of masses, radii, and hydrogen atom. Section 13 examines the dynamics of the electron-shell in metals, insulators, liquids, and vacuum. Section 14 introduces Ulianov's reformulation of Maxwell's equations based on membrane kinematics.

Overall, this work shows that UST provides a coherent geometric framework from which atomic structure, particle properties, electrodynamics, photon generation when protons and electrons for hydrogen atoms, and electron behavior in different media and materials emerge naturally.

Historical Background of Atomic Models

The modern picture of the atom emerged through a sequence of bold proposals faced with decisive experiments. The first influential twentieth–century model was **Thomson's** "plumb pudding" which treated the atom as a positively charged diffuse sphere with embedded electrons to neutralize the charge. Although it offered a simple route to global neutrality, it could not explain discrete spectral lines nor scattering at large angles [1].

A critical turning point occurred with **Rutherford**'s analysis of the Geiger–Marsden gold–foil experiments. A small fraction of α particles were deflected through large angles, an observation incompatible with a diffuse positive charge [2]. Rutherford concluded that nearly all the mass and positive charge reside in a compact nucleus, with electrons occupying the surrounding space, implying that the atom is mostly empty [3]. This led to a planetary atom model, an analogy with a solar system, where protons are reunited in a solid central *nucleus*, orbited by high-speed electrons forming an electron cloud or electrosphere

In order to reconcile atomic stability with line spectra, **N.,Bohr** introduced quantized orbits for the hydrogen atom: electrons occupy stationary states with angular momentum restricted to integer multiples of $\hbar$. In this model, the allowed radii and energies are [4].

$$r_n = a_0, n^2, \qquad E_n = -\frac{13.6\ \text{eV}}{n^2} \quad (n = 1,2,3, \ldots), \tag{1}$$

where the Bohr radius a_0 is

$$a_0 = \frac{4\pi\varepsilon_0\hbar^2}{m_e e^2} \approx 0.529, \text{Å}. \tag{2}$$

Bohr's postulates successfully reproduced the Balmer series and established a quantitative bridge between structure and spectra, even as the picture of classical orbits soon gave way to wave mechanics.

However, attempts to measure simultaneously the position and velocity of an electron bound to the atomic nucleus were unsuccessful. This limitation is explained by the **uncertainty principle**, formulated by **W. Heisenberg**, which places kinematic bounds on the simultaneous knowledge of non-commuting observables such as position and momentum [5].

$$\Delta x, \Delta p \geq \frac{\hbar}{2}. \tag{3}$$

This principle is not a statement about experimental imperfections but an intrinsic feature of quantum kinematics. It undercuts the classical notion of well-defined electron trajectories inside atoms and motivates a shift from orbit pictures to state vectors and operators.

Based on this concepts, **E.,Schrodinger** introduced wave mechanics, in which the electron is described by a complex-valued wavefunction $\psi(r,t)$ evolving via the Schrodinger equation [6].

For stationary states of hydrogen, separation of variables yields orbitals labeled by quantum numbers *n,l,m*, with characteristic radial and angular structures. **Born** provided the statistical interpretation: $|\psi|^2$ gives the probability density for finding the electron in space upon measurement. In this view, what earlier drawings depicted as a "cloud" is not a material shell, but a probability density shaped by the potential and boundary conditions [7]. The interpretational shift was dramatized by **Schrödinger**'s "cat" thought experiment, highlighting the role of measurement and decoherence in connecting quantum superpositions to classical outcomes [8].

In textbook hydrogen, the lowest s orbital has a spherically symmetric density, while higher shells introduce nodal surfaces and directional structure. The patterns provided by Schrödinger's wave-equation solutions match the observed selection rules and spectral intensities.

In summary, the picture of an electron as a pointlike corpuscle moving in a classical orbit was replaced by the wavefunction description, in which the electron is represented by a quantum state whose modulus squared yields a spatial probability density (with units of C/m^3 when interpreted as charge density). Upon interaction/measurement, this probability distribution *appears* to "collapse," producing outcomes consistent with a localized particle carrying the full elementary charge Q_e. Note that this differs conceptually from a literal cloud of microscopic charges around the nucleus: if such charges were distinct classical particles, mutual Coulomb repulsion would disperse them, which is not what is observed.

Ulianov String Theory

The Ulianov Theory introduces a new type of string theory, called *Ulianov String Theory* (UST) [9,10]. UST is built upon a complex and discrete notion of time,

$$s=t+iq,$$

where the real time component t is an integer multiple of the Planck time t_P, and the imaginary time component q advances through a fixed number of "processing steps" equal to N_S (the number of Simoon, $N_S=7.77\times10^{60}$). Each step corresponds to a fundamental "small sphere", and the full set of N_S spheres forms a string-like structure analogous to a necklace of Planck-scale beads.

In this framework, each "small sphere" corresponds to an Einstein–Rosen–Ulianov bridge, a *Ulianov wormhole* (UWH). One mouth of the UWH appears as a Planck-diameter sphere that moves in imaginary time at imaginary light speed, advancing by one Planck length per unit of Ulianov imaginary time,

$$U_T = \frac{t_P}{N_S} = 6.9385 \times 10^{-105}\ \text{imaginaryseconds}.$$

Along its trajectory in imaginary time, the UWH can rotate in both space and time and can change its mass and electric charge. For any observer unable to access or perceive imaginary time (such as humans in real spacetime), the imaginary dimension collapses. As a consequence, the single 5D pointlike UWH manifests in real spacetime as a 4D *Ulianov String* composed of N_S sequential copies of the same UWH state. The resulting object resembles a necklace of Planck-scale pearls, each capable of assuming positive or negative mass and electric charge.

This string can coil or fold into higher-dimensional structures, naturally forming 2D membranes, 3D shells, or even 4D hypersurfaces within spacetime.

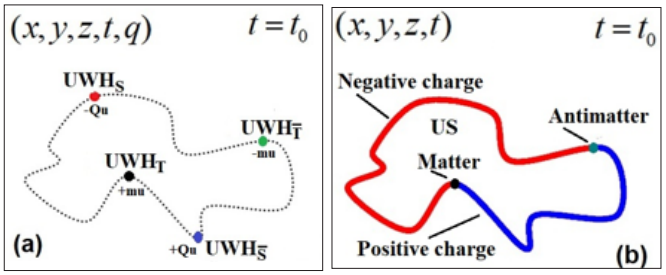

Figure 1: The foundation of Ulianov String Theory: the collapse of imaginary time transforms a single Ulianov Wormhole into an Ulianov String. (a) The UWH travels at imaginary light speed and may change its type along the path. (b) The resulting Ulianov String (US) is obtained after the collapse of imaginary time.

Within this model, all known particles in our universe, including leptons, baryons, quarks, and photons, are constructed from specific combinations of UWHs that fold into characteristic strings and membranes. These structures determine the observed mass, charge, spin, and interaction properties of each particle species. The application of UST over the protons electrons and neutrons string/membranes model led to the Ulianov Atomic Model (UAM) [11].

Application of Ulianov String Theory

Ulianov String Theory (UST) is built upon two fundamental entities called UWHs (Ulianov Wormholes). Conceptually, the UWH model [9] extends the classical Einstein–Rosen bridge idea: each UWH behaves as a tiny bridge or tube connecting two regions of two subuniverses that are separated by walls of space or time.

In our universe, a UWH is effectively observed as a sphere of Planck-scale diameter (L_P) that exists within a five-dimensional kinematic structure governed by complex time,

$$s=t+i\,q,$$

so that its evolution unfolds simultaneously in real time t and imaginary time q.

The cornerstone of UST is the following mechanism: a single UWH traveling at constant speed in imaginary time, when viewed by an observer who cannot perceive the q dimension, undergoes a *collapse of imaginary time*. This collapse makes successive imaginary-time positions of the UWH appear simultaneously in real time. The result is a chain of N_S identical UWHs connected in sequence (an Ulianov string) analogous to a necklace made of N_S Planck-sized beads.

Such a string has:

- a total length $N_S\ L_P$,
- an effective membrane area $N_S\ L_P^2$ when folded into a 2D surface,
- and a 3D volume $N_S\ L_P^3$ when compressed into a volumetric object.

In this section, we explore how the geometry of Ulianov strings allows them to be folded, rolled, or wrapped into higher-dimensional structures. By rolling the string into a compact three-dimensional configuration, one obtains a solid membrane sphere, the proton prototype. By folding it into a thin two-dimensional surface, one obtains a spherical shell, the basic structure of the electron.

Kinematics in Complex Time.

Evolution proceeds in discrete imaginary-time "processing steps". At each step the UWH may hop by one L_P in space or one T_P in time, tracing closed paths in (x,y,z,t) as q advances. This admits a constant unit-speed constraint that couples spatial and temporal hopping:

$$V_{ex}\,(q)^2+V_{ey}\,(q)^2+V_{ez}\,(q)^2 = V_e\,(q)^2,$$

$$\left(\frac{V_e(q)}{c}\right)^2 + V_t(q)^2 = 1,$$

with $V_e\in\{-c,0,+c\}$ (one L_P per T_P along a chosen axis) and $V_t\in\{-1,0,+1\}$ (one T_P step) at each q-tick.

Because the microscopic speed is fixed and unitary in this sense, an observer who does not resolve q perceives an effective *collapse*: the UWH "smears" into a *string* made of many beads of L_P-diameter. The number of beads equals the total imaginary-time length measured in the processing steps.

Cosmic Complex-Time Geometry

The complex time s is represented by a cylinder whose base (t=0) hosts pure q-evolution (a frozen real time akin to a cosmological inflation stage). As t grows, the cylinder flares into a cone. A simple model is

$$T_i = t_{i0}+t,$$

Where T_i is the length of imaginary time axes in seconds (or imaginary seconds) and t_{i0} It's how much imaginary time grew at the base of the complex time cylinder, while real time was still frozen. This means that, at the present cosmic age t=$T_U\simeq 4.35\times10^{17}$ s (13.8 BY), if t_i0 is negligible, the imaginary time extent is $T_i\approx TU$ and the *Simoon number* (N_S), related to the number of "processing steps" made by the imaginary time loop (or the number of spheres in one Ulianov string) can be defined as:

$$N_S = \frac{T_i}{T_P} \approx 8.07\times10^{60}$$

counts the total processing steps (or, equivalently, the number of L_P beads in an extremely long necklace).

Each T_P completes one q-cycle, which defines an *Ulianov Imaginary Time quantum*

$$T_{IU} = \frac{T_P}{N_S} \approx 6.67\times10^{-105}\ \text{s}.$$

Two UWH species and their quanta.
Each bead (UWH) comes in two species:

- UWH_T (*time-wall* wormholes, carriers of inertial-gravitational mass), with unit *Ulianov* mass

$$m_U = \frac{2\pi P_M}{N_S} = 1.76 \times 10^{-68} \text{ kg}, \quad (4)$$

recognizing positive or negative sign;

- **UWH_S** (*space wall* wormholes, carriers of electric charge), with unit *Ulianov charge*

$$q_U = \frac{2\pi Q_E}{N_S\sqrt{\alpha}} = 1.51 \times 10^{-78} \text{ C}, \quad (5)$$

Including positive or negative sign.

Ulianov Force Scale
At a separation of exactly one Planck length L_P, both the mass–mass attraction (like-sign m_U) and charge attraction (opposite-sign q_U) share the same *Ulianov force* magnitude,

$$F_U = 7.91\times10^{-77}\ N\ (d=L_P), \quad (6)$$

so that in UST the fundamental gravitational and electric force intensities are matched at the bead scale.

Why Electromagnetism Dominates Macroscopically.
UWH_T quanta arise only when the string completes full turns, so the population of mass-carrying beads is proportional to the number of completed windings, approximately

$$N_T \sim \frac{N_S L_P}{L_{\text{turn}}}, \quad (7)$$

with L_{turn} the circumference per winding. The remaining (dominant) beads are UWH_S, i.e., charge carriers. Consequently, although the microscopic force scales match at L_P, the macroscopic world exhibits much stronger effective electromagnetic interactions than gravitational ones, simply because $N_S \gg N_T$ and the *abundance* of UWH_S far exceeds that of UWH_T.

Particles as Single-Bead Engines
In UST every observable particle (photons, electrons, protons, neutrons) corresponds to a *single* UWH that cycles through space and time once per imaginary-time tick. When q collapses, the trajectory becomes a string of fixed total length that can wrap into 2D membranes or 3D bodies in space-time. Particles that do not rotate in real time (so their complete string is not a 4D membrane, but only a 3D membrane) will reside within one real time digital frame (defined in only one Planck time Δt). For this kind of particles, the UWH dynamics can be observed in an analogy with a 3D printer extruding identical beads at fixed rate for a fixed duration: many printers (particles) can operate in parallel to produce diverse 2D/3D shapes, but if any shape is unrolled, the string length equals the same bead count.

In this 3D–printer analogy, as one UWH can have only one property (mass or electric charge) that can be only positive or negative, four possible values (+m_U,-m_U,+q_U,-q_U) can be seen as the 3D-printer nozzle can extrude beads of L_P diameter that can be represented by four types of "colors", each encoding one UWH property:

- Red bead: negative electric charge ($-q_U$) (UWH_S),
- Blue bead: positive electric charge ($+q_U$) ($\overline{UWH_S}$),
- Black bead: positive mass ($+m_U$) (UWH_T),
- White bead: negative mass ($-mU$) ($\overline{UWHT}$).

Printed 2D/3D figures are therefore predominantly red/blue (charge carriers), with sparse black/white micro-features (mass carriers). Furthermore, the figures present several emergent properties of their membranes wrapping shapes that can be basically:

- **Photons:** 4D cylinders extended in space and real time as a single indivisible object, but we observe only time-slices of this Cylinder (3D cylinders cut in time by the "sharp knife" of by the present time line) composed of interlaced red/blue ribbons (like a barber shop rotating lollipop), with fine black/white filaments threaded along the ribbons' cores.
- **Electrons:** two equivalent renderings: (i) a red spherical shell with Planck length thickness and a small black "dot" near a pole; or (ii) a red spherical cap with a thin black rim filament.
- **Protons:** two equivalent renderings: (i) a solid blue sphere with a black line (a small cylinder) from a pole to the interior; or (ii) a hemisected blue solid sphere with a black disk wth Planck length thickens sealing the cut.
- **Neutrons:** two equivalent renderings: (i) a black coin with same proton radii and Planck length thickness (ii) a black cylinder almost equal to the proton mass cylinder.

Closure and Discretized Radii.
Every figure must close with the last bead touching the first. Hence allowed radii/diameters occur in discrete steps so that shells and cylinders complete exact windings. For solid spheres (viewable as onion-like nested shells), the radius can vary only within bounds set by inter-layer spacing.

Physical Implications (Departures from Standard Models)

- All material quanta (including light) are strings of equal length; mass/energy differences arise from how many windings are allocated to shell vs. core paths.
- Electric charge and mass are not uniformly smeared: charge predominantly inhabits extended shell/ribbon regions (red/blue), whereas mass localizes as coins, short rods, or extremely thin lines (black/white).
- Antimatter carries negative mass $-m_U$ composed by $\overline{UWH_T}$. So the antimatter "figures" will be like same as the matter ones, but with white beads instead of black beads and changing blue beads by red beads.
- A photon balances $+m_U$ and $-m_U$ mass filaments with a total mass equal to zero but with internal inertial retaining kinetic energy and be affected by gravitational fields.

Behavior of Overlapping UWH
When UWH units are placed side by side, their masses or electric charges add linearly, and no significant distortion of spacetime is produced. However, when UWH_T (the mass-carrying type) overlap (a natural process, since UWH_T attract each other) the resulting configuration generates a layered spacetime deformation analogous to the concentric structure of an onion. Each additional overlapping UWH_T produces a complete new "shell" of geometric distortion.

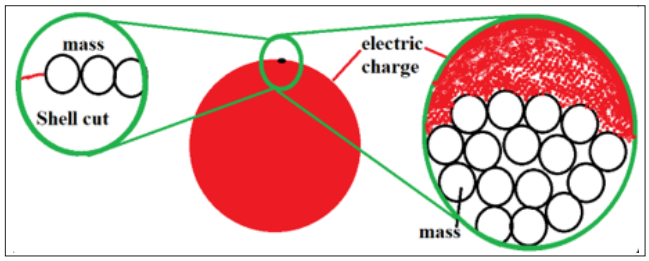

Figure 2: Structure of the electron membrane in UST. The black circles represent mass–carrying wormholes UWH_T, each with mass $+m_U$, responsible for generating the localized mass pole of the electron. The red points represent charge–carrying wormholes UWH_S, each with electric charge $-q_U$, whose radius is 11.7 times smaller than that of UWH_T.The left magnification shows a cut of the spherical shell, highlighting the linear chain of UWH_T that forms the mass pole. The right magnification shows a surface patch of the membrane, where densely distributed UWH_S (red) sit above a packed layer of UWH_T (black), revealing how charge is spread over the shell while mass remains concentrated at a single polar region.

Thus, N overlapping UWH_T generate a spacetime distortion equivalent to placing N^3 UWH_T side by side on a spherical membrane.

Depending on the membrane on which the system resides, its total diameter (or scale), and its rotation rate, two distinct physical effects may arise:

- In some configurations, a cluster of N UWH_T behaves as an effective mass increase m_U N^3, leading to an energy increase N^3 m_U c^2. In this case, the total weight could in principle be measured on a physical scale.
- In other cases, the spatial distortion corresponds geometrically to a mass-like increase m_U N^3, but without any increase in actual energy. The membrane adjusts its radius and rotational frequency so that the physical energy remains N MU c^2. A laboratory scale in this case would measure a mass close to Nm_U rather than N^3 m_U, even though the geometric deformation corresponds to an effective mass N^3 m_U

It should be noted that the spacetime deformation produced by overlapping UWH $_T$ can be interpreted as the formation of micro black holes (or nano black holes, for systems with mass smaller than m_P). In the context of Ulianov Theory, this mechanism reproduces the equations of black holes and also allows one to deduce Newton's law of gravitation [12,13]. However, in UT the interpretation is different from Einstein's proposal that matter curves space by "shrinking" it locally. Instead, UT states that the presence of UWH_T *locally increases the effective Planck length* (and Planck time), causing measured spatial distances to appear smaller and the flow of time slower, thereby producing the observed phenomena of spatial contraction and gravitational time dilation [14].

When UWH_S (the charge-carrying type) overlap (which only occurs under external forcing or confinement, since UWH $_S$ repel each other) the resulting deformation resembles the behavior of soap bubbles when pressed together. To preserve the total membrane area, the effective total charge is reduced. Instead of producing a charge N q_u, a cluster of N UWH $_S$ produces an effective charge $Q_{eff}=\sqrt{N}\ q_u$, meaning that charge decreases when UWH $_S$ are superimposed.

Therefore, although UWH $_S$ also distort spacetime (changing the L_P and t_p values), the distortion produced by N overlapping UWH S scales only as √N, whereas for UWH _T it scales as N^3.
This fundamental asymmetry, combined with the fact that UWH_S resist unification while UWH_T strongly prefer clustering, historically led modern physics to consider that only mass can distorted the space time and that electric charges do not produce distortions, when in fact the presence of charger in the electron membrane for instance generate Planck lengths multiped by a 11.7 factor, that small in compassion with the factor of 137 of P_L increase (increase of volume by 137^3) generated by the electron mass. But if we observe the complete electron shell, a presented in figure (2) where the mass area is only a small dot the mean P_L increasing will be equal to 11.7, the value generated by the electron charges.

The UST Photon Model

A basic aspect of UST is that the mass of a membrane is determined by the number of windings with which the membrane is wrapped. The mass of any membrane M_x is given by

$$M_x=N\,m_U$$

where N is the number of windings, equal to the total length of the string divided by the average winding length λ_x:

$$N=\frac{N_s P_L}{\lambda_x}.$$

Thus,

$$M_x=\frac{N_s P_L m_U}{\lambda_x}.$$

For the photon, which has a simple cylindrical geometry, this results in:

$$M_f=\frac{h}{2\pi c\,\lambda},$$

since

$$E_f=\frac{hc}{2\pi\lambda},$$

$$M_f=\frac{E_f}{c^2}=\frac{h}{2\pi c\lambda}.$$

For the smallest possible photon, corresponding to the Planck wavelength,

$$\lambda=P_L,$$

we obtain:

$$M_f=\frac{h}{2\pi c P_L}=M_P,$$

which is the Planck mass.

In UST, for the same configuration we have:

$$M_x=\frac{N_s P_L m_U}{2\pi P_L}=\frac{N_s m_U}{2\pi}.$$

Since

$$m_U = \frac{M_P}{N_s}\, 2\pi,$$

we find

$$M_x = \frac{N_s m_U}{2\pi} = \frac{N_s}{2\pi}\left(\frac{M_P}{N_s} 2\pi\right)$$

$$M_x = M_P.$$

Thus, for the smallest possible photon, both models yield the same mass, and it is straightforward to show that this equivalence holds for any wavelength. From the UST perspective, the photon is not merely an oscillating point-like excitation but a four–dimensional geometric object. Figure (3) shows a spatial snapshot of this structure: a cylindrical membrane of length λ along the z-axis and radius λ/2π in the *x*–*y* plane, propagating at the speed of light. Inside this cylinder, the electromagnetic fields arise from the internal rotation of the UWH chain that composes the photon.

However, this spatial cylinder is only a *three-dimensional slice* of the full object. In UST the photon is a 4D hypercylinder whose extension in the time dimension has height T=λ/c, corresponding to one wave period. Thus, what we commonly call "the photon at the present instant" is simply the intersection between the full hypercylinder and the present-time hypersurface.

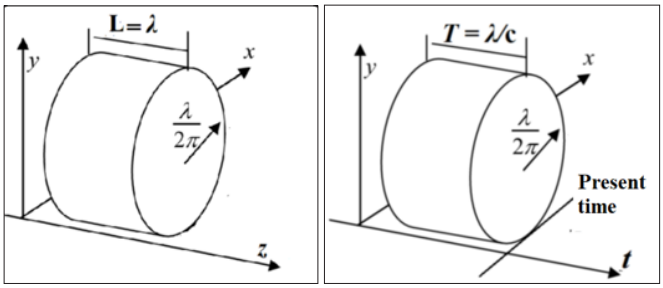

Figure 3: Geometric representation of a photon in UST. Left: three-dimensional spatial cylinder of length λ and radius $\lambda/2\pi$, moving along the z-axis. Right: the same object including its temporal extension, forming a four-dimensional hypercylinder of height $T=\lambda/c$ in real time. The usual photon observed in the present time framework, corresponds to a 3D slice of this full 4D structure.

Photon Mass and Energy in UST

In UST, a photon is produced when the Ulianov string wraps into a cylindrical membrane. Each circular cross-section of this cylinder forms a loop that naturally divides into two semicircular arcs:

- one containing positive electric charges (UWH_S^- with aligned $+q_U$),
- one containing negative electric charges (UWH_S with $-q_U$).

At the midpoint of the positive arc lies a UWH_T with positive mass m_U (a matter mass point), and at the midpoint of the negative arc lies a UWH_T^- with negative mass $-m_U$ (an antimatter mass point).

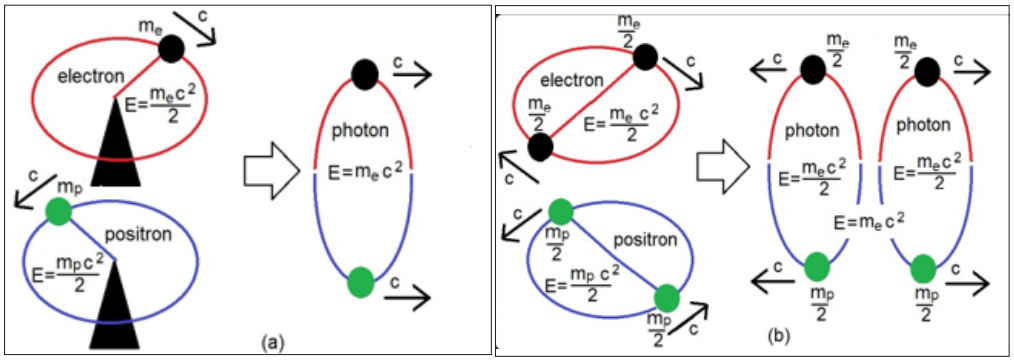

Figure 4: Mass conservation model: rotational kinetic energy transforms into translational kinetic energy. (a) Simplified representation of the electron and positron storing rotational kinetic energy. (b) Photon formation from electron–positron annihilation, where rotational kinetic energy is converted into translational kinetic energy.

Because the total Ulianov string length is fixed at $N_s P_L$, and because exactly one mass point appears per circular turn, the photon mass satisfies

$$M_f = \frac{N_s P_L}{\lambda} = \frac{\hbar}{\lambda c}.$$

The antimatter component has the same magnitude and opposite sign.
As illustrated schematically in Figure (4), Einstein's relation

$$E=Mc^2$$

acquires a new interpretation in UST. It becomes a conversion of rotational kinetic energy (stored in the internal motion of the mass poles around the circular section) into translational kinetic energy (carried by the photon as it propagates at speed *c*).

In this picture, the electron and positron masses are not destroyed during annihilation; they merge to form the photon. Matter and antimatter remain present inside the photon, but with opposite signs, yielding zero net mass while each component individually moves at the speed of light.

The internal kinetic energy of each mass pole is

$$E_k = \frac{|m|c^2}{2},$$

which gives the total photon kinetic energy:

$$E_{kf} = \frac{M_f c^2}{2} + \frac{|-M_f|c^2}{2} = M_f c^2.$$

Before annihilation, the electron and positron rotate tangentially at speed c, storing rotational kinetic energy

$$E_{ce} = \frac{m_e c^2}{2},$$

$$E_{cp} = \frac{|m_e| c^2}{2},$$

each photon produced carries half of each contribution.

Thus, UST does not describe annihilation as "mass destroyed", but as the release of rotational kinetic energy into translational kinetic energy. A classical analogy is a ball rotating on a cord: when the cord is cut, the ball moves linearly with the same kinetic energy, although mass itself is unchanged. Rotational motion in a closed space cannot perform external work, whereas linear motion through space can generate impacts, release energy, or even cause damage. This illustrates how matter may be viewed as "frozen light", while light may be seen as matter in motion without any real loss of total mass in the system due to the pairing of matter with antimatter.

The UST Electron Model

In UST, the electron is modeled as a string composed of two kinds of Ulianov wormhole: small quantities of UWH_T, a UWH in time walls that has positive mass, and a larger number (a N_S number) of UWH_S,a UWH in space walls that has negative electric charge.

Furthermore, in the Ulianov Atomic Model (UAM), a framework built upon Ulianov String Theory, electrons are not point-like particles but extended membranes formed by the collapse of imaginary time [11]. Before observation, an electron consists of a single Ulianov wormhole (UWH) propagating through complex time. After the collapse of the imaginary-time dimension, its N_S UWH copies appear simultaneously, forming a closed string of fixed length $N_S\, L_P$, which folds into a thin Planck thickness spherical shell.

This shell model differs from the standard wave–particle duality, but remains fully compatible with the successful predictions of modern quantum mechanics. In the conventional interpretation, the wave function ψ encodes a probability distribution to locate a point-like electron. In UST, the same Schrödinger equation instead describes a *real* charge-density field (units of C/m^3) distributed over the spherical membrane. The familiar "electron cloud" becomes a physical, oscillating membrane rather than a statistical abstraction.

A central feature of UST is that **all the rest mass of the electron is concentrated in a tiny polar region** of the shell, a "polar mass" which behaves as a point-like corpuscle without electric charge. This localized mass rotates at the speed of light around the symmetry axis, fixing a *unique intrinsic rotation sense* for all electrons. What physicists call "opposite spin" simply corresponds to the same rotating shell viewed upside down, with the polar mass located at the opposite pole. This picture removes spin paradoxes while preserving all measurable spin phenomena.

As illustrated in Figure 5, UST admits two geometric realizations for the electron membrane:

- a **thin spherical shell** of negative charge, with Planck-length thickness and a radius ranging from tens of picometers to several nanometers, depending on the energy level, and hosting a "small circle" area (the electron polar mass) at the North pole of the electron shell that contains all the electron mass;
- a **hemispherical-cap configuration** that appears only inside atoms, where two caps join to form a complete shell and the polar mass relocates along the equatorial rim.

These two shapes differ only in geometry, not in the underlying microstructure. In bound states, the cap geometry arises because two electrons in the same orbital come into mass-contact along the equatorial line. The distance between their polar-mass points becomes one Planck length, generating a strong gravitational contact force, enhanced by a factor of $1/L_P^2$, which exceeds their electrostatic repulsion by several orders of magnitude. Because the two electrons touch their mass points, one shell is necessarily upside down relative to the other; although both maintain the same absolute rotation sense, they appear to have opposite spins [15]. This provides a natural explanation for why atomic orbitals require electron pairs with opposite spins, without invoking the Pauli exclusion as a purely abstract rule.

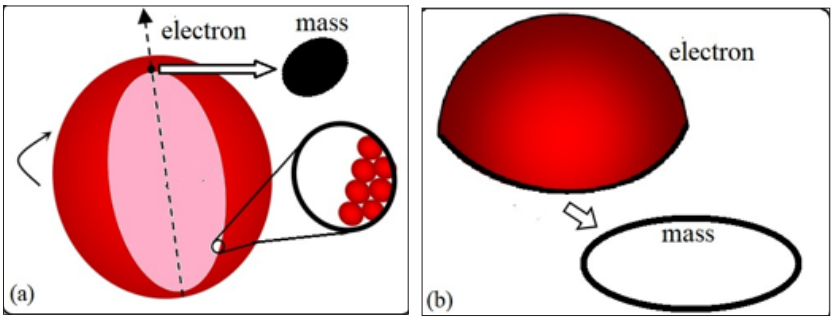

Figure 5: Electron geometries in UST: (a) a thin spherical shell with a polar mass that fixes the common spin sense; (b) a hemispherical cap where the mass relocates coherently along the equatorial rim in bound states.

Within this geometry, electric and magnetic phenomena acquire a unified microscopic origin. A rotating charged shell naturally produces a magnetic dipole moment, and because all electrons share the same intrinsic rotation sense, large groups of them can align under very small external fields. What is usually interpreted as "electric currents that generate magnetic fields" becomes, in this view, the collective ordering of many preexisting microscopic magnetic fields carried by each electron.

A crucial prediction of UST is that a free electron maintains its spherical-shell form with a radius of roughly $R_e \approx 5.1$ nm, but this large radius appears only for an electron essentially at rest (spinning but with small translational velocity).

In particular, a 5 nm electron shell radius coincides with:

- the Bohr radius for highly excited hydrogen states ($n \sim 10$);
- the de Broglie wavelength of a very low-energy electron accelerated by ~0.1 V.

Thus, free-electron diffraction, double-slit interference, and electron-microscope wave behavior arise naturally from extended-shell geometry, which explains the electron wave–particle duality: the polar mass behaves as a particle, while the oscillating shell behaves as a wave.

In the quantum-wave model, the act of observation collapses a probability distribution into a localized electron. In the UST framework, imaginary time exists continuously, but an observer (who cannot perceive this dimension)induces a collapse of the imaginary time coordinate. However, in UST an electron does not collapse into a point containing all of its mass and charge. Instead, it manifests as a rotating spherical shell with a large radius, with electric charge distributed across the membrane and the rest mass concentrated at a single polar region. A stationary electron shell (only rotating) may have a radius of approximately 5 nm, however, when inserted into atomic hydrogen, the shell interacts elastically with the proton, shrinks, acquires additional mass through UWH clustering, and reproduces Bohr-like radii and energy levels with excellent numerical accuracy. Likewise, when the electron shell is accelerated to high velocities, its relativistic mass increases and the radius contracts to a scale comparable to the de Broglie wavelength of the moving electron.

Figure (6) highlights a key structural feature of the Ulianov Atomic Model: electrons belonging to the same orbital touch each other's mass poles, generating a very intense Strong Gravitational Contact Force (SGCF), whereas electrons belonging to different orbitals never touch and experience only Coulomb repulsion. This fundamental distinction explains why electrons pair tightly inside a single orbital, but orbitals repel each other radially, producing the stable nested-shell geometry of atomic electron clouds. A direct numerical comparison clarifies why the SGCF completely dominates the dynamics inside a single orbital. The Coulomb repulsion between two electrons separated by the Bohr radius is obtained from

$$F_E = \frac{e^2}{4\pi\varepsilon_0 r_{\text{Bohr}}^2}$$

and yields

$$F_E = 8.2 \times 10^{-8}\ \text{N}.$$

In contrast, the gravitational contact force between the two mass poles touching at one Planck length is computed as

$$F_G = \frac{G\, m_e^2}{L_P^2},$$

giving

$$F_G \approx 2.1 \times 10^{-1}\ \text{N}.$$

Thus, SGCF is millions of times stronger than electric repulsion. This quantitative result explains why the electron caps pair can be connected inside a single orbital, forming a unique sphere with total spin null because although Coulomb forces tried to separate the electrons, the SGCF keeps them together. Note that electrons shells and caps in different orbitals repel each other but maintain a stable equilibrium because the force fields are radial and tending only to shrink the internal electrons and expand the external ones.

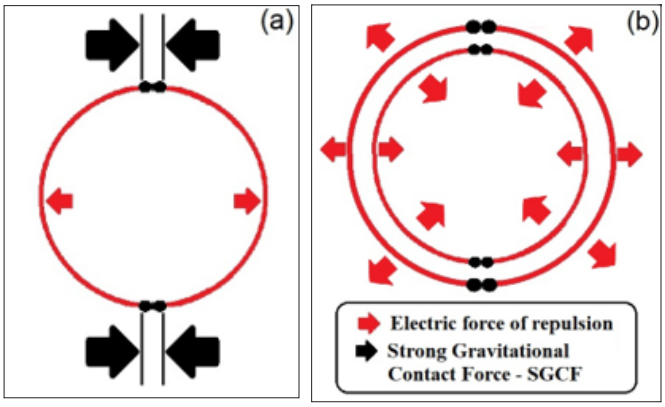

Figure 6: Forces acting on electrons in the Ulianov Atomic Model. (a) Two electrons sharing the same orbital: their mass poles remain in direct contact and the Strong Gravitational Contact Force (SGCF) dominates the interaction, exceeding the electric repulsion by many orders of magnitude. (b) Electrons in different orbitals do not touch their mass poles; only shell–to–shell electric repulsion occurs, pushing the outer orbital outward and compressing the inner orbital inward. Nested spherical shells ("Russian doll" structure) enhance repulsion but remain far weaker than the SGCF acting within a single orbital.

The electron-shell geometry emerging from UST also naturally leads to a new organizational scheme for atomic electrons: the Ulianov Electron Distribution (UED). As shown in the companion work, this distribution reproduces Pauling-like orbital filling with high fidelity while providing a more geometrically grounded rule set tied to the structure of the nucleus. The UED model further clarifies metallic bonding by predicting the number and spatial orientation of electrons with free mass-poles, offering a physical mechanism that explains why different metals form distinct crystalline and conductive behaviors [16].

The UST Proton Model

In UST, the proton is modeled as a string composed of two kinds of Ulianov Wormholes: small quantities of UWH_T, a UWH in time walls that has mass properties, generating positive mass and a larger number (N_S number) of UWH_{TST}, a sequence of tree UWH (in time wall- space wall- time wall) that has positive electric charge properties and null mass.

As presented in Figure (7), in the UST, a proton string can be wrapped in two ways:

- A solid sphere composed of spherical layers forming an onion structure. In this model, the proton mass is represented by the UWH_T that forms a circle in each onion spherical layer, so the total proton mass can be seen as a cylinder. If we consider an analogy where the proton is like a blue billiard ball, we use a drill to make a hole, radial to the center of the ball, placing a cylindrical body inside this hole, representing the proton mass.

- A solid half sphere (spherical cap) composed of spherical layers of the cap that form an onion structure. In this model, the proton mass is represented by the UWH_T forming a ring in each spherical cap layer, so the total proton mass can be seen as one circle with a Planck length thickness. If we consider an analogy where the proton is like a blue billiard ball, we cut the ball in half and paint the resulting circle in black, representing the proton mass.

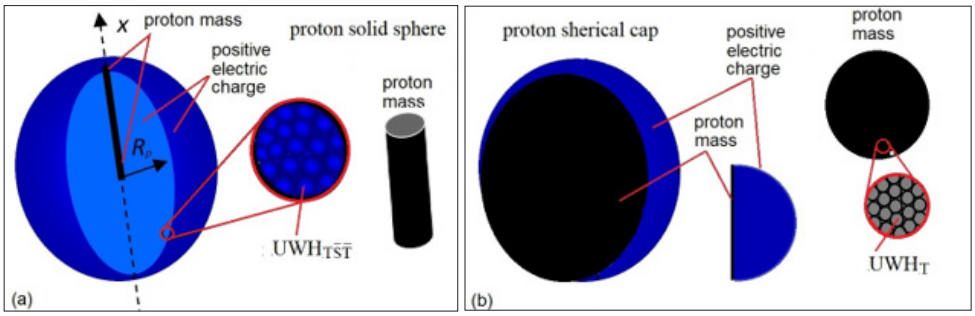

Figure 7: Proton model in the Ulianov String Theory: a) Proton forming a solid sphere composed of $UWH_{\overline{TST}}$ that contain electric charge, with the proton mass composed of UWH_T, forming a small cylinder over the proton radius in the proton North Pole. b) Proton forming a solid half sphere with its mass distributed over a disc with one Planck length thickness.

The proton configurations obtained in UST are fully consistent with previous analyzes showing that proton geometry naturally organizes into a hierarchical "Kepler–Ulianov Proton Tree" (KUPT), where layered proton packing and SGCF-based connections uniquely determine the minimum stable isotopes observed in nature [17, 18]. These independent results reinforce that the UST proton is not an ad-hoc construct but a geometric unit from which a nuclear structure emerges directly.

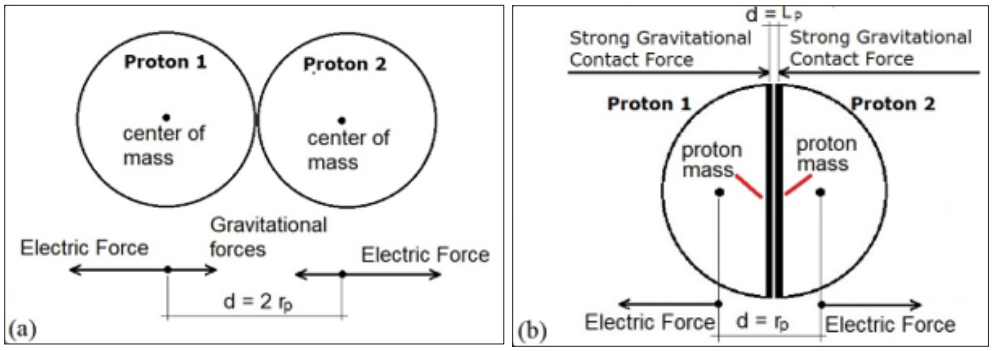

Figure 8: a) Standard representation of two protons within the helium nucleus and the forces acting between them (the neutrons are excluded to simplify the model). The mass and electric charge are distributed over all proton spheres, and the distances between masses and charges are the same. b) UST representation of two protons within the helium nucleus and the forces acting between them (the neutrons are excluded to simplify the model). The electric charge is distributed over all proton caps, and the mass is distributed over a disc. The distances between the two charges are equal to the proton radius, and the distance between the two masses is equal to the Planck length. This configuration generates a Strong Gravitational Contact Force that is two thousand times greater than the electrical repulsion force.

Calculating Proton Properties

In this section we compute the masses and radii of the proton and the electron within the UST framework. A useful analogy is to imagine two pearl necklaces, each pearl having a diameter of 1 cm and each necklace being 100 m long (thus containing N_S=10,000 pearls).

To construct a proton, the necklace is wound in successive circular layers—much like the layers of an onion, forming a solid sphere built from rings of increasing radius. If the winding is sufficiently compact, the final sphere has volume

$$V_p = \frac{4}{3}\pi R_p^3,$$

which must match the number of pearls multiplied by the volume of each individual pearl.

For the electron, the process is fundamentally different: the necklace is wrapped into a *spherical shell*. The area of this shell,

$$A = 4\pi R_e^2,$$

must equal the number of pearls multiplied by their effective surface contribution, since the electron is modeled as an ultra-thin membrane rather than a solid body.

Although this analogy is simple, the real calculation involves several complications:

- The string may be folded N times before winding; In this analogy where the string has a length of 100 m, if N=5, only 20 m of string effectively participate in the winding.
- The packing behavior is different for UWH $_T$ (mass carriers) and UWH$_S$ (charge carriers): mass units tend to overlap, whereas charge units tend to spread apart.
- Each fundamental unit may be treated either as a sphere of radius L_P or as a cube of side L_P. When forming volumes or surfaces, these units may pack densely (filling the region completely) or only touch at discrete points, leading to effective areas and volumes larger than the simple sum of the individual units.

These factors determine the precise calculation of proton and electron radii. For the masses, we adopt two complementary models:

- For the proton, the mass is distributed in a s**olid spherical region**, with density determined by the three-dimensional overlap of UWH $_T$. Most of the overlap is moderate (on the order of only a few units) thus space-time distortion is small and the resulting geometry is closer to an ideal sphere.
- For the electron, the mass is concentrated along an **equatorial line** of length equal to the circumference of the shell, with thickness 1 L_P, but with **137 overlapping turns**. This high degree of overlap produces strong space-time distortion and significantly deforms the spherical shell.

Because mass and charge distort space-time, the ideal shapes (solid sphere for the proton and spherical shell for the electron) undergo relativistic corrections. The electron is the most extreme case: its mass concentrated at a single pole produces distortions generated by 137 superposed UWH$_T$. For the proton, the UWH$_T$ overlap is distributed throughout the volume and corresponds to roughly five units, yielding much smaller geometric distortion and a nearly ideal sphere.

Thus, despite being motivated by a simple analogy, this approach allows the fundamental properties of the proton and electron to be derived quantitatively from universal geometric constraints imposed by the total string length $N_S L_P$ and its folding patterns.

Proton Radius Value from a Simplified UST Geometry

A first observation allows us to model the proton as a shell composed of N_s/137 spheres, wrapped into a solid sphere whose total volume satisfies:

$$R_{xp}^3\left(\frac{4}{3}\pi\right) = \frac{N_S}{N_C},$$

so that:

$$R_{xp} = \left(\frac{N_S/137}{(4/3)\pi}\right)^{1/3}.$$

This R_{xp} is expressed as a number of Planck spheres and must be multiplied by P_L to obtain a physical radius:

R_p=R_{xp} P_L=3.90154×10^{-16} m=0.46 R_p muonicvalue.

Although this value is approximately half of the standard proton radius, it confirms that the geometric framework is functional and only requires refinement.

The factor (4/3)π arises when packing cubes inside a sphere; however, UST involves packing spheres inside a larger sphere, which behaves more like packing cubes inside a cube (in the sense that the effective packing factor is closer to 1). Under this simplification, the relation becomes

$$R_{xp}^3 = \frac{N_S}{N_C},$$

and therefore:

Rp=Rx PL=(N_s/137)$^{1/3}$ P_L=6.28926×10^{-16} m=0.76 R_p muonicvalue

This smaller value arises because the proton mass and the overlap of charge units produce a space-time distortion (an effect not included in this simplified calculation). Even so, obtaining an error of only 24% using such a basic geometric model indicates that starting from the age of the universe it is possible to recover the number of spheres in the string that forms the proton, first wrapped into a structure of size 1/α and then wrapped into the solid sphere that determines the proton radius.

Since the calculation uses only two well-established parameters and produces a purely theoretical prediction with a remarkably correct order of magnitude, this suggests that the model is indeed capturing some real and deeper geometric characteristic of the proton.

Proton Mass in a simplified Spherical-Cap Model

In the cap model, the proton mass is accumulated in a disk of unit thickness containing approximately $\pi Rx\ P^2$ spheres. Thus, the mass is:

$$M_{xp}=m_U\ \pi R_x^2$$

Using the UST relations:

$$M_{px} = \frac{2\pi M_{Pl}}{N_s}\pi\left(\left(\frac{N_s}{137}\right)^{1/3}\right)^2 = 8.16191\times10^{-29}\ \text{kg} = \frac{1}{20}M_P standard.$$

This is 20 times too small because the calculation does not include the mass increasing when UWH$_T$ are superimposed. Since in the proton sphere this overlap is approximately $\sqrt[3]{137}$ units, we will have:

$$M_{px} = \frac{2\pi M_{Pl}}{N_s}\left(\left(\frac{N_s}{137}\right)^{1/3}\right)^2 * 137/2 = 1.757\times10^{-26}\ \text{kg} = 0.95M_P standard.$$

Note that in this equation, the factor π has been replaced by a factor of 1/2, which is due to the cap-shaped proton model considering a radius divided by 2, generating a final factor π/4, which, due to the packing of spheres in a spherical area, generates a factor of 1/2.

Proton Radius and Mass from the UST Packing Rules

In Ulianov String Theory (UST), the mass of a particle is determined by the number of loops in which the fundamental string is wrapped. This number is equal to the total length of the string (N_s L_P) divided by the circumference of the loop, which depends on the radius of the membrane being formed. Consequently, small-radius configurations correspond to heavy particles (the proton case), while large-radius configurations correspond to light particles (the electron case).

As a direct result, each type of wrapping satisfies a proportionality relation where the product of particle mass and particle radius yields a constant:

$$M_f R_f = K_f \frac{\hbar}{c},$$
$$M_P R_p = K_p \frac{\hbar}{c},$$
$$M_e R_e = K_e \frac{\hbar}{c},$$

where M_f and R_f are the photon mass and wavelength, M_P and R_p are the proton mass and radius, and M_e and R_e are the electron mass and radius. Empirically, one finds:

$$K_f = 1,$$
$$K_p = 4,$$
$$K_e = (4N_C)^{3/2},$$

where N_C=137 is the number of layers in the electron shell,

Thus, applying the proton relation,

$$M_P R_p = \frac{4\hbar}{c},$$

we obtain refined expressions for the proton mass and radius within the UST context.

Proton Radius

The proton radius can be calculated using the following equation:

$$R_p = \left(\frac{N_S/\pi^3}{(4/3)\pi}\right)^{1/3} \left(\frac{4\pi}{3}\right) \frac{P_L}{\pi}.$$

which can be written in a more compact form as:

$$R_p = \left(N_S \frac{16}{9\pi^4}\right)^{1/3} P_L.$$

For the optimized value N_s=7.77×10^60, this gives:

R_p=8.4282×10^{-16} m=1.0011 R_p muonicvalue.

corresponding to an error of only 0.11%.

In this formula, the term:

$$R_{xp} = \left(\frac{N_S}{(4/3)\pi}\right)^{1/3}$$

represents the radius in units of Planck spheres. The factor π appears as a packing coefficient for 3D sphere arrangements (associated with π^3), and the factor P_L/π is related to the increase of the effective Planck length due to the space-time distortion produced by the proton's mass and electric charge.

For the mass component alone, the scaling factor should be approximately 5.15 (equal to $\sqrt[3]{137}$) and for the charge component it should be about 2.26 (equal to $\sqrt{51.15}$, but numerically the value π best reproduces the combined effect.

Proton Mass

For the proton mass, the corresponding UST equation is:

$$M_P = \frac{2\pi\, PM}{N_S}\, 2\pi \left(\left(\frac{N_S}{(4/3)\pi}\right)^{1/3}\right)^2.$$

which can be expressed more compactly as:

$$M_P = PM \left(\frac{36\pi^4}{N_S}\right)^{1/3}.$$

For the optimized value N_s=7.77×10^{60}, this yields:

$$M_P = 1.669 \times 10^{-27}\ \text{kg} = 0.99811\ M_P^{\text{standard}}.$$

corresponding to an error of only -0.18%.

In this equation, the factor $2\pi PM/N_S$ represents a unit mass, while

$$\pi \left(\left(\frac{N_S}{(4/3)\pi}\right)^{1/3}\right)^2$$

represents the number of spheres in the circular area over which the string is wrapped to generate a solid spherical membrane. An additional factor of 2 is included, obtained by empirical adjustment.

The errors in these expressions are quite small because the chosen value Ns=7.77×10^{60} (corresponding to a Universe age of 13.23 billion years) was selected slightly below the theoretical value 8.07×10^{60} (associated with the commonly cited age of 13.8 billion years). We believe that the current estimate of the age of the Universe may contain an uncertainty larger than ±0.1BY (since it is given with only one decimal place), possibly reaching ±0.5BY.

It is important to observe that the above equations reproduce the expected UST relation

$$M_P R_p = \frac{4\hbar}{c}.$$

Since the factors Ns cancel out in the final relation, this empirical development appears to compensate for space-time distortion effects and yields remarkably precise values.

For comparison, using the standard-cosmology value Ns=8.07×10^{60} gives

$$M_P = 1.6483 \times 10^{-27}\ \text{kg} = 0.9854\ M_P\text{standardvalue},$$

and

$$R_p = 8.562 \times 10^{-16}\ \text{m} = 1.014\ R_p^{\text{std}}.$$

Thus, even when adopting the conventional Universe age, the calculated proton mass and radius remain close (less than 1.5% of error) to the experimentally known values.

Electron Analysis

In the case of the proton, the UST model produces results that are very close to those obtained by the standard framework, making the comparison relatively easy to understand and accept. For the electron, however, the discrepancy is much greater when viewed from the perspective of the traditional point-particle model, which describes the electron as an extremely small object orbiting the nucleus at high angular velocity. In contrast, the wave-function description introduced by Schrödinger brings the standard model significantly closer to the spherical-shell geometry proposed by UST.

Although these aspects were briefly mentioned in the introduction, the discussion there was necessarily fast and superficial. In this

section, we return to the electron in a more rigorous and detailed way, examining how its membrane-like structure, radius, mass distribution, and dynamical behavior emerge naturally from the geometric rules of Ulianov String Theory.

Standard Electron Model

As described at the beginning of this article, current physics treats the electron within the wave–particle duality framework:

- Around the nucleus, the electron behaves as a wave composed of electromagnetic fields, modeled by Schrödinger wavefunctions. In the hydrogen atom, this appears as a spherical probability cloud representing the charge-density distribution.

- When the electron is observed or interacts with any measurement device, the probability distribution of the wavefunction collapses, and the electron becomes a point-like particle carrying all mass and charge within a radius effectively zero (typically between 10^{-18} and 10^{-22} m).

- When ejected from the nucleus, the electron again behaves like a wave and can, for example, pass through a double slit. But upon interacting or being observed, the wavefunction collapses once more into a point-like particle.

This dual model works well, but as with the photon wave–particle duality, many conceptual mysteries remain unresolved.

UST Strings Behavior

Within this scenario, UST proposes that the "collapse" of the electron wavefunction is not a collapse of probabilistic information caused by the act of observation, but rather a "collapse of imaginary time", also triggered by observation.

In UST, imaginary time truly exists and evolves in discrete cycles that correspond to processing steps, each one lasting an extremely small interval (Ulianov Time: $t_U \approx 6.9\times10^{-105}$ imaginary seconds). However, for an observer who exists only in real time and cannot perceive imaginary time (such as human beings), the very act of observing produces a "collapse of imaginary time."

Before observation, the *Ns* UWH composing an electron exist as isolated Planck-scale spheres (with diameter of P_L) along a trajectory in imaginary time. After the collapse, these *Ns* UWH appear simultaneously, forming a continuous closed string composed of *Ns* spheres.

If placed in a straight configuration, these spheres form a string of length $Ns\ P_L$ meters, while in a 2D membrane of thickness P_L, they occupy an area:

$$A = N_s P_L^2 \quad \mathrm{m}^2,$$

and in a 3D solid membrane, a volume:

$$V = N_s P_L^3 \quad \mathrm{m}^3.$$

Adjacent spheres are connected by the UWH trajectory in imaginary time; effectively, there exists an unbreakable link or infinitely strong constraint connecting each UWH to its two neighbors.

Because identical charges repel, a string of UWH defining a US (Ulianov String) forms a perfect circle that minimizes repulsion forces. For a US carrying only one type of charge, each complete turn closes onto a single mass point. If the string includes two semicircles of opposite charge, they naturally contact each other, and the midpoint of each semicircle produces a mass point.

Thus, circular turns align in space and form cylinders, with each turn touching two mass points. The lateral surface of the cylinder becomes a 2D membrane where UWH_S of opposite charge remain bound despite repulsion between consecutive rings.

Similarly, rolling a 2D membrane into a cylindrical spiral results in several concentric cylinders. If their bases are connected and sufficient internal pressure is applied, even though interaction forces develop between each cylindrical layer, the circular symmetry makes the average radial force effectively zero. Consequently, the cylindrical structure remains stable, and UWH arranged in 3D structures can form cubic blocks without dispersing.

Therefore, the fact that UWH of the same charge can form continuous lines, areas, and volumes despite mutual repulsion can be explained in two complementary ways:

- Each UWH exists as an isolated particle following a trajectory in imaginary time. In this regime, no repulsion occurs because at each imaginary-time step only one charge exists, and its path advances by "skipping" one sphere in space or time.

- After the collapse of imaginary time, the full set of *Ns* UWH experiences repulsive forces, but the configuration remains bound in lines or membranes. Repulsion inflates these membranes and shapes them into circles, cylinders, or spheres depending on how their boundaries are connected.

Alternative Paths in the Historical Evolution of Atomic Models

Let us imagine that, at the time of J. Thomson, when he realized that the atom was almost entirely empty space, he had chosen a different analogy. Suppose that instead of discarding the "plum pudding" idea of a diffuse negative cloud and adopting a solar-system analogy, Thomson had modeled the hydrogen atom as a soap bubble: a solid proton at the center (concentrating all mass and positive charge) surrounded by an extremely thin spherical membrane representing the electron.

In such a model, it would make no sense to attempt to measure a point-like position for the electron. Consequently, there would have been no experimental motivation to formulate Heisenberg's uncertainty principle. Furthermore, since a "soap-bubble electron" oscillates and ripples, it would be natural to describe it using a wavefunction whose output is a real charge-density field in C/m^3, rather than a probability density of charge distribution.

If this "bubble electron'' were expelled from the atom, the natural behavior would be for the membrane to retain its shape while expanding dramatically in size, rather than collapsing into a point-like particle.

From a physical standpoint, there are two mutually exclusive possibilities:

A: The electron truly is a wave–particle dual entity.

B: The electron is a negative spherical shell that behaves like a wave, but contains a tiny mass point at one of its poles, giving rise to particle-like behavior.

If hypothesis **B** were true (even if only with very small probability) it becomes important to note that the historical interpretations of Thomson and Bohr would naturally push the scientific community toward hypothesis **A**. Observing a spherical membrane

and misinterpreting it as a tiny high-speed point would almost inevitably lead to the planetary-orbit analogy, and thus to the dual model, even if the dual model were not fundamentally true.

Therefore, one may argue that modern physics did not adopt Model A because it is the only possible model, but rather because the planetary-system analogy (instead of a soap-bubble analogy) may have been fundamentally misleading. The analogy produced questions that were themselves misguided:

"What is the position and velocity of the electron orbiting the nucleus?"

Although this question be invalid (because we cannot attributed a point position to a membrane), some physicists were actually very smart and arrived at the correct answer even starting from the wrong question:

"It is impossible to measure simultaneously the position and velocity of the electron with precision, therefore we should model it as a probability wave surrounding the nucleus".

The author therefore appeals to the physics community to consider the implications of UST. Despite its unusual origins (Einstein–Rosen–Ulianov bridges, or Ulianov Wormhole, interpreted as unit-charge or unit-mass Planck-scale spheres traveling along imaginary-time trajectories which, once collapsed, produce strings of fixed length N_s P_L) the resulting physical description closely matches the dual wave–particle electron model.

However, UST provides this agreement **without requiring duality**. The wave-like and particle-like properties emerge naturally from the collapse of imaginary time and the internal geometry of UWH clustering, removing conceptual paradoxes and simplifying the interpretation of electron behavior.

Electron Mass Calculation

To calculate the electron mass we may consider the following expression:

$$M_e = 2\pi \frac{P_M}{N_s}\ 2\pi \left(\frac{N_s}{4\pi}\right)^{1/2} 137^3 \cdot 4, \qquad (8)$$

In this formula:

- The factor $2\pi\ P_M/N_s$ defines the unit mass contribution,
- R_{xe}=(Ns/(4π))$^{1/2}$ is the effective radius produced when the N_s spheres are arranged in a spherical shell (ignoring layer overlap),
- 2πR_xe is the circular equatorial ring that represents the mass distribution in the spherical-cap electron model,
- The factor 4 arises because the observed R_{xe} comes from the spherical shell, while the mass in the cap model involves a doubled radius and two UWH_T grouped into a double ring.

Equation (8) can be written in compact form as:

$$M_e = P_M\ 8 \left(\frac{\pi^3}{N_s}\right)^{1/2} 137^3.$$

Using the optimized value N_s=7.770×10^{60}, (which means the universe is 13.23 billion years old instead of 13.8 billion, which is a 5% error in the current value, something that could be happening) we obtain:

$$M_e = 8.94366067 \times 10^{-31}\ \text{kg} = 0.98180752\ m_e^{\text{std}} \quad (\text{error} \approx 1.8\%).$$

Note that if we use the N_S value given by:

$$N_s = \frac{T_U}{T_P} = 8.07 \times 10^{60},$$

we obtain:

$$M_e = 8.77456655 \times 10^{-31}\ \text{kg} = 0.964\ m_e^{\text{std}}\ (\text{error} \approx 3.4\%).$$

The error produced by this equation is small, but bigger than the errors observed in proton mas equation using the N_S optimized value. This indicates that this formula is valid but not yet fully corrected for geometric subtleties. One important source of deviation is the distortion of the spherical shell produced by the mass concentration at one of the poles presented in figure (2), introducing an intrinsic error of order ∼1.8% even when the optimized value of *Ns* is used.

Calculation of the Electron Radius

In the previous sections, we presented formulas for computing M_P, R_P, and M_E based on the Simoon number N_s and on the winding factor 137=1/*α*, which is directly associated with the number of overlapping layers in the spherical electron shell. These formulas rely essentially on geometric definitions of length, area, and volume for circles and spheres and, within the UST framework, yield physically coherent interpretations. Their results can be directly compared to the standard values of M_E, M_P, and R_P, notwithstanding the well known controversy in the proton radius: the value extracted from ordinary hydrogen spectroscopy is about 4% larger than the value obtained from muonic hydrogen.

However, in the case of the electron radius the situation becomes much more complex. In the standard wave–particle duality model, the "particle" electron would have an extremely small radius (much smaller than that of the proton) possibly in the range of 10^{-18} m to 10^{-20} m. By contrast, the "wave" electron surrounding a hydrogen nucleus in the s orbital forms a thick spherical distribution whose size is comparable to that of the entire electron cloud.

In the Bohr model, the particle-like electron occupies circular orbits defined by

$$R_0 = n^2\ a_0,$$

where n is the principal quantum number (n=1,2,3,…) and a0 is the Bohr radius, approximately 5.29×10^{-11} m. Thus, for n={2,3,...,10} we obtain the following:

$$R_0 = \{\ 2.1 \times 10^{-10},\ 4.7 \times 10^{-10}, \ldots,\ 5.3 \times 10^{-9}\ \}\ \text{m},$$

demonstrating that the increase factor of n^2 can generate a very large orbital radius in the Bohr model.

Although pedagogically useful for one-electron systems, the Bohr model was ultimately replaced by modern quantum mechanics, in which electrons are described not by fixed circular orbits but by probability clouds (wavefunctions). In this picture, the electronic cloud of an isolated hydrogen atom has no sharp boundary, making it impossible to define or measure an absolute "radius" for a single hydrogen atom because the electron retains a non-zero probability of being found arbitrarily far from the nucleus.

However, the Bohr radius was not abandoned, as it represents the most probable distance in the ground state and is still referenced as the effective radius of the hydrogen atom. But it is not a physical boundary and does not mean that the atom "actually" has that radius.

A real measure of experimentally accessible hydrogen is the *covalent radius,* approximately 37 pm. It is defined as half the internuclear distance between the nuclei of two identical hydrogen atoms bonded in an H_2 molecule. Techniques such as X-ray diffraction and rotational spectroscopy determine the internuclear separation to be about 74 pm, yielding the covalent radius of 37 pm, which is interpreted as the effective electron-cloud radius in molecular hydrogen.

Because this value (37 pm) is only slightly smaller than the Bohr radius (52.9 pm), the Bohr ground-state prediction remains consistent and represents the lowest-energy configuration when a proton and electron combine to form hydrogen, emitting a photon of energy 2.17×10^{-18} J.

If the atom absorbs 5.4 J (approximately one-quarter of the binding energy released in hydrogen formation), the electron transitions to the n=2 orbital, whose radius is four times larger. With the appropriate amount of energy, the electron reaches higher and higher orbitals until, at the limit of 2.17×10^{-18} J, the electron becomes unbound and escapes the proton.

In the Bohr model, for n=10 we obtain an orbital radius of

$$R_{10}=100\ a_0=5.29\text{ nm}.$$

Even though modern quantum mechanics does not assign a strict maximal radius to the s orbital, it is reasonable that the spherical electronic cloud defined by the ground-state wavefunction has a mean radial extent close to 52.9 pm (which is indeed the accepted effective radius for an isolated hydrogen atom in its lowest energy state).

In this context, if the n=10 state indeed exists and the Bohr model remains valid as a limiting approximation, then the corresponding electronic cloud would extend to approximately 5.29 nm.

What is the Size of the Electron Outside the Nucleus?

This raises an important question: when the electron is expelled from the atom, does its cloud disappear and the wave collapse into a point-like particle? Experiments such as the double-slit experiment and the operation of electron microscopes themselves demonstrate that the electron continues to behave as a wave. Thus, even when free, the electron still exhibits an extended spatial structure (a "cloud'' associated with variations of electric charge density), and can, for example, pass through two slits simultaneously.

For an electron outside the nucleus moving as a wave, quantum mechanics assigns a de Broglie wavelength given by

$$\lambda=\frac{h}{p}=\frac{h}{m_e v_e}.$$

In electron microscopes, the electron is accelerated by a voltage V, giving it a kinetic energy

$$E_C=VQ_e,$$

with momentum

$$p^2=Vm_eQ_e.$$

Thus,

$$\lambda=\frac{h}{\sqrt{Vm_eQ_e}}.$$

For voltages

$$V=\{\ 0.1\text{ V},1\text{ V},10\text{ V},100\text{ V},1\text{ kV},10\text{ kV},100\text{ kV}\ \},$$

we obtain approximate electron wavelengths:

λ={ 5.48 nm,1.73 nm,0.54 nm,0.173 nm,54.8 pm,17.3 pm,5.48 pm }.

A striking convergence appears when comparing these values with high-energy Bohr orbitals. For example, in the Bohr level n=10, the electron cloud has a radius of approximately 5.3 nm and can be removed from the atom with only ~0.136 V. An electron accelerated by 0.136 V has a de Broglie wavelength of about 4.7 nm.

For n=20, the Bohr radius becomes 21 nm with an ionization energy of only 0.034 V, producing a de Broglie wavelength of about 9.5 nm. However, for extremely large n, the models diverge: for n=100, the Bohr radius becomes 529 nm, while the required ionization energy drops to 0.00136 V, giving a de Broglie wavelength of only 47 nm, leading to inconsistent values between the models, probably because the Bohr model is not valid for so large n values

Thus, the models only agree in a limited physical regime. For n~10, both descriptions converge to characteristic length scales of the order of a few nanometers, around 5 nm.

The hypothesis proposed by the author is that a free electron may indeed be approximated by a spherical structure of radius ~5 nm, which can equivalently be interpreted as a cylinder of height 5 nm and radius 5 nm, a geometry directly related, in UST, to the cylindrical structure that models the photon.

Why the Electron Wraps into Multiple Layers

In the UST model, the factor $1/\alpha$=137 is directly associated with the electron being a spherical shell composed of 137 overlapping layers. A similar effect also exists in the proton, but because the proton is already a solid sphere, the overlapping dissolves into an effective compression equivalent to only 5.15 layers.

UST explains that this multilayer wrapping arises from a competition between mass and electric-charge effects inside the proton sphere and inside the electron shell. Focusing on the electron, where this effect is most evident:

- Electric repulsion between identical charges would favor a very large spherical electron with only one layer.
- Mass effects, however, increase with the number of turns, and increase even more with volumetric overlap. Thus, mass prefers a smaller spherical shell with the largest possible number of layers.

A direct comparison between electrical repulsion and mass attraction is not possible because in a multilayer shell, the electric

fields from adjacent layers partially cancel each other.
An analogy helps clarify this:
Consider a cylinder formed by rolling a sheet into multiple turns, sealing the top and bottom, and applying air pressure inside. If the cylinder has ten turns and the pressure is large but constant: Radial pressure tends to unwind the cylinder (because with only one turn the radius increases and the internal pressure drops). However, radial forces cannot generate tangential forces required to roll or unroll the cylinder because these directions are orthogonal.

Thus, if friction between layers is negligible, even a small tangential force can roll the cylinder tighter, increasing the internal pressure. In the same way, gravitational (mass) forces (though much weaker than electric forces) act in the appropriate tangential directions to wrap the electron, while electric forces act radially.

Since the full equilibrium calculation depends on unknown microscopic factors, we instead observe a fundamental fact: **the proton and electron have equal charge**, and therefore their strings undergo the same number of folds, 137.

Thus, the mass-driven wrapping in the proton (solid sphere of radius R_p) may be compared to the mass-driven wrapping in the electron (spherical shell of radius R_e).

A Simple First Estimate
We can divide the proton mass and electro mass by two and consider the gravitational forces that advance between these half masses when separated by the particle radius:

$$F_{GP} = \frac{(m_p/2)^2 G}{R_p^2},$$
$$F_{GE} = \frac{(m_e/2)^2 G}{R_e^2},$$

and, also propose one equilibrium equation:

$$F_{GP} = K_1 \; F_{GE},$$

where the value K_1 is a function of the length of the string and is directly proportional to the value N_S. In addition to that, as the number of layers N_C increases with the value N_s, the value K_1 also is directly proportional to the value N_C.

Using known values of m_p, m_e, and R_p, and assuming R_e=5 nm, we obtain the following:

$$K_1 = \left(\frac{N_C}{4}\right)^{1/3},$$

yielding

$$R_e = \frac{m_e}{m_p} R_p \left(\frac{N_s}{4}\right)^{1/6}.$$

For $N_s = T_U/T_P = 8.07\times10^{60}$:

$$R_e = 5.15 \times 10^{-9} \text{ m}.$$

For the optimized value $N_s = 7.77\times10^{60}$:

$$R_e = 5.12 \times 10^{-9} \text{ m}.$$

This value means that for $R_e = 5.12\times10^{-9}$m , a value of N_C=137 can also be obtained based on the equations above.

A More Refined Comparison
A more sophisticated comparison uses the volume of the proton sphere and the area of the electron shell, yielding the following relation:

$$\frac{(R_p/P_L)^3}{N_s}\frac{8}{(4/3)\pi}\frac{1}{m_p^2} = \frac{(R_e/P_L)^2}{N_s}\frac{\pi}{4}\frac{1}{m_e^2}.$$

Remarkably, N_s cancels out:

$$\frac{(R_p/P_L)^3 8}{(4/3)\pi} = \frac{(R_e/P_L)^2\pi}{4}\left(\frac{m_p}{m_e}\right)^2.$$

Solving for R_e gives:

$$R_e = \sqrt{\frac{24}{\pi}}\frac{m_e}{m_p}\frac{R_p^{3/2}}{P_L^{1/2}} = 5.15986\times10^{-9} \text{ m}.$$

These closely matching values strongly suggest that within UST, when an electron is expelled from an atom and brought to rest in empty space, it assumes the form of a spherical shell with radius of approximately 5.1 to 5.2 nm. This is consistent with:

- a high-n Bohr orbital radius,
- and the de Broglie wavelength of a very low-energy electron (e.g., accelerated by 0.1 V), which is also of order 5 nm.

UST Formula for the Free Electron Radius
Once a valid estimate for the spherical-shell electron is established, UST provides a direct formula:

$$R_e = \left(\frac{N_s}{137(4\pi)}\right)^{1/2}\frac{P_L}{137}\frac{2}{\pi}.$$

where the N_s spheres are folded 137 times, giving an area:

$$4\pi R_x^2 = \frac{N_s}{137}.$$

To convert R_x (number of spheres) into meters, we multiply by P_L/137 because the electron shell has a distorted metric where P_L is effectively inflated by 137 (reducing real distances by a factor of 137).

The factor 2/π corresponds to a packing correction of (4/π)/2 associated with sphere tiling on a surface.
For $N_s = 7.77\times10^{60}$ we obtain:

$$R_e = 5.142\times10^{-9} \text{ m}$$

in excellent agreement with all previous estimates of the free (with low velocity) electron spherical shell radius.

Generation of the Hydrogen Atom in UST
In UST, mass is proportional to the number of windings of the underlying string: for a fixed string length, smaller radii correspond to higher masses, while larger radii correspond to smaller masses. Figure (9) shows that when a proton enters the spherical shell of an electron, the total charge is neutralized and a new force arises between the positive UWH _T of the proton and the negative UWH _T of the electron.

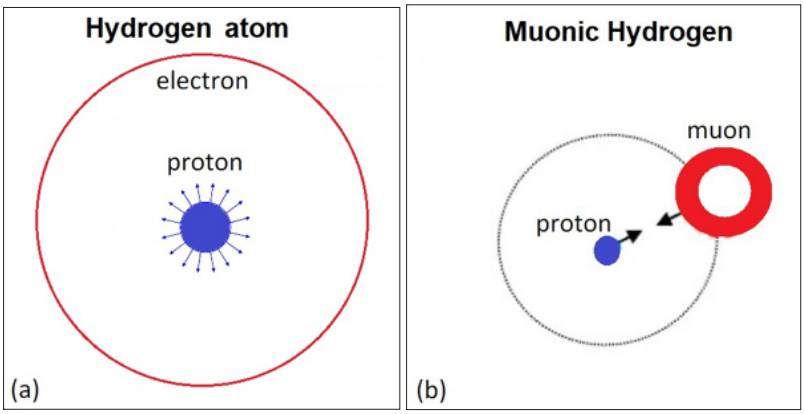

Figure 9: The proton radius variation in the hydrogen atom: a) In the hydrogen atom (represented in a 2D cut), the electron's negative charges exist in a large spherical shell (with the size of the atom) and attract the proton sphere's positive charges in all directions, causing the proton radius to increase. b) In muonic hydrogen (represented in a 2D cut), the muon's negative charges attract the proton sphere's positive charges in only one direction, so the proton radius does not increase.

This is fundamentally different from placing a positive point charge inside a negatively charged hollow sphere. In the classical case, external forces on the surrounding positive charges remain unchanged. In UST, however, when the proton enters the electron shell, the external forces vanish: each UWH_S of the proton becomes elastically paired with a corresponding UWH_S of the electron, producing a spring-like interaction:

$$F_i = k\, d_i = \frac{q_U^2}{4\pi\varepsilon_0 d_i}\, d_i.$$

Where q_U is a Ulianov unitary electric charge (q_U=1.51×10^{-78}C).
These elastic forces create several important effects:

- They stabilize a configuration with the proton at the center of the electron shell (spherical mode).
- They stabilize a configuration with the proton at the base of the spherical cap of the electron (cap mode).
- The internal state of the proton (sphere or cap) determines the corresponding state of the electron.

Because the proton experiences stretching forces, its radius increases as if it were an onion whose layers separate slightly. A larger radius means fewer windings, and therefore the proton becomes lighter and expels UWH_T (mass emission).

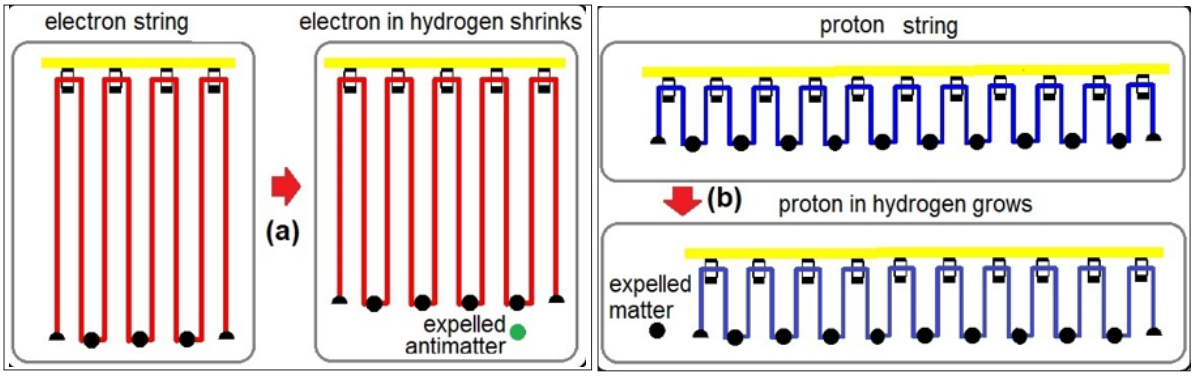

Figure 10: Curtain–loop analogy for the electron string inside hydrogen. (a) A free electron has a longer effective loop length. (b) When the electron enters the hydrogen atom, its string wraps more tightly, the number of loops increases, and the electron mass effectively grows, expelling a small amount of antimatter (green circles).

The electron, as presented in Figure (10), experiences the opposite effect: forces compress its shell, decreasing the radius, increasing the mass, and requiring additional UWH _T. These are obtained from virtual pairs in vacuum (matter–antimatter). The electron thus absorbs matter and expels antimatter.

Figure (11) illustrates that expelled proton matter and expelled electron antimatter combine to form a photon.

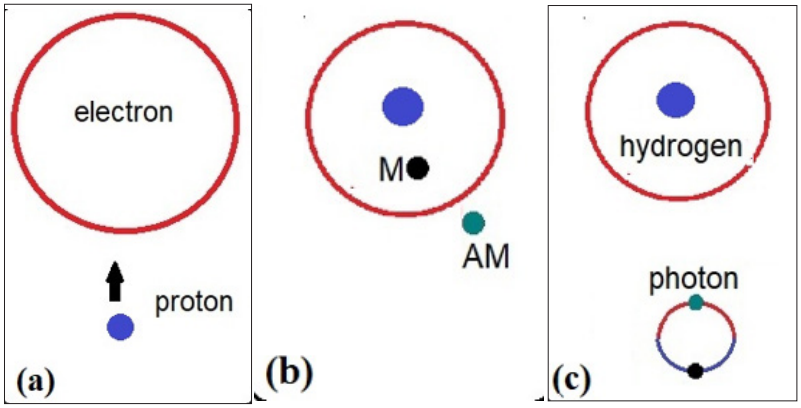

Figure 11: Formation of the hydrogen atom with a photon emission. (a) A free proton has a compact wrapping with shorter loop extent. (b) When forming hydrogen, the proton expands slightly, reducing the number of loops, which corresponds to the expulsion of ordinary matter (black circles). (c) The combined adjustments of electron and proton strings expel matter and antimatter in complementary amounts, naturally generating a photon during hydrogen formation.

Radius Shifts During Hydrogen Formation

Given the photon energy E_f, we compute its equivalent mass $M_f=E_f/c^2$. Using the previously established UST relations:

$$M_P R_p = \frac{4\hbar}{c},$$

$$M_e R_e = (4N_C)^{3/2}\frac{\hbar}{c},$$

with N_C=137.

Thus:

$$R_e = \frac{(4N_C)^{3/2}\hbar}{cM_e}.$$

After the electron absorbs additional mass from hydrogen formation, $M_e \rightarrow M_e+M_f$. However, in the electron shell, masses stack in 137 overlapping layers, magnifying the geometric distortion:

$$M_f \longrightarrow M_f\,137^3.$$

Thus:

$$R_{eh} = \frac{(4N_C)^{3/2}\,\hbar}{c\,(M_e+M_f 137^3)}.$$

So, the electron radius in hydrogen becomes:

$$R_{eh}=7.13438\times10^{-11}\ \text{m}=1.34\ a_0.$$

For the proton:

$$R_{ph} = \frac{4N_C\,\hbar}{c(M_P-M_f 137^3)}.$$

With E_f=2.685×10^{-18} J and M_f=2.42×10^{-35} kg:

$$R_{ph}=8.73803839\times10^{-16}\ \text{m}$$

which is 1.038 R_p muonic, very close to the measured hydrogen value R_p=8.768×10^{-16} m.

The Kepler Ulianov Proto Tree

The use of the Strong Gravitational Contact Force (F_{SGC}) in the UST model can also explain the need for neutrons to make stable nucleons. This allows for the definition of various proton-neutron structures, such as the UPD (Ulianov Proton Dumbbell), and UPPB (Ulianov Proton Pogo-Ball), presented in Figure 12-a), These structures are basic building blocks that can be united to construct atomic nucleons, forming a 3D structure named the KUPT [17] (Kepler Ulianov Proton Tree), as shown in Figure 12 for the Oganesson atom nucleon with 118 protons. This is the maximum number of protons that the KUPT structure can accommodate, which coincidentally is the maximum number of protons in a known element. Interestingly, each full layer of the KUPT corresponds to a noble gas atom: Helium, Neon, Argon, Krypton, Xenon, Radon, and Oganesson.

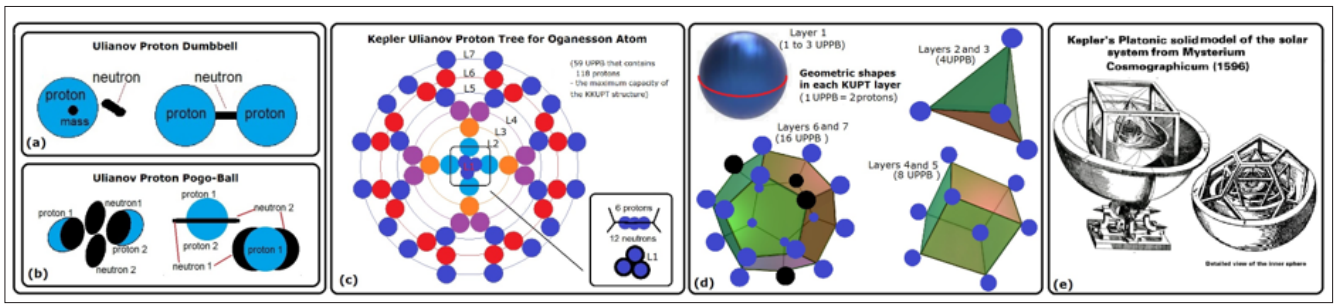

Figure 12: Proton model in the Ulianov String Theory: a) Ulianov Proton Dumbbell. b) Ulianov Proton Pogo-Ball. c) Kepler Ulianov Proton Tree for the Oganesson Atom. The colors were used only to facilitate the visualization of the layers. d) 3D shapes of the KUPT; each blue sphere represents one UPPB that contains two protons. The geometric figures help to define each UPPB in 3D space. e) Kepler's second model for the orbit of planets in the solar system; the platonic solid organization proposed by Kepler is the same observed in the KUPT layers: Sphere, tetrahedron, cube, and dodecahedron.

Ulianov Electron Distribution and its Relation to the Pauling Scheme

In standard quantum chemistry, electronic structure is organized according to the Pauling (or Aufbau) principle, where orbitals (*s,p,d,f*) determine the number of valence electrons and, consequently, the bonding capacity of each atom. Although highly successful, this scheme treats electrons as point-like entities occupying probability clouds with no direct geometric connection to the internal structure of the nucleus.

In Ulianov String Theory (UST), the situation is fundamentally different. The nucleus is not a featureless point but a highly structured three-dimensional *Kepler–Ulianov Proton Tree* (KUPT), built layer-by-layer through short-range gravitational-contact interactions. The geometry of each completed KUPT layer determines the allowed electron-shell geometries outside the nucleus. Thus, in UST the *nucleus commands the electron distribution*, not the reverse. This yields a new electron counting scheme (the *Ulianov Distribution*) that naturally accommodates g and h shells and predicts the number of electrons that possess free, mass-bearing poles capable of participating in chemical or metallic bonding.

In this picture, each electron is a spherical shell whose mass pole must align with an available direction determined by the nucleus. Complete KUPT layers correspond to noble gases, while partially filled outer layers determine the number and orientation of "open" electron mass-poles. The correspondence with chemical behavior emerges directly from geometry rather than from empirical filling rules.

Comparison Between Pauling and Ulianov Distributions

The following table compares the Pauling electron distribution with the Ulianov electron distribution for four representative metals. The complete 118-element mapping can be found at [16]. This small sample already shows that each Pauling configuration has a clear counterpart in the Ulianov scheme, but the logic behind the two notations is fundamentally different.

A useful analogy is to imagine labeling rooms in a large hotel. Pauling notation assigns floor and room numbers according to the traditional (*s,p,d,f*) orbital scheme. This works well, but in some regions the sequence appears irregular—much like a hotel built around a spiral ramp where adjacent rooms may unexpectedly "jump" from one floor to another.

The Ulianov distribution, on the other hand, is based on the geometric structure of the nucleus itself (the KUPT layers). Because these layers grow continuously and systematically, the Ulianov numbering follows a smooth, uninterrupted sequence—eliminating the need for auxiliary rules, exceptions, or memorized "little tables." The electron configuration emerges naturally from geometry rather than from empirical filling patterns.

Element	*PaulingDistribution*	*UlianovDistribution*
Fe(26)	$1s^2\ 2s^2\ 2p^6\ 3s^2\ 3p^6\ 4s^2\ 3d^6$	$1s^2\ 2s^2\ 2p^6\ 3s^2\ 3p^6\ 4s^2\ 4g^6$
Cu(29)	$1s^2\ 2s^2\ 2p^6\ 3s^2\ 3p^6\ 4s^2\ 3d^9$	$1s^2\ 2s^2\ 2p^6\ 3s^2\ 3p^6\ 4s^2\ 4g^9$
Ag(47)	$1s^2\ 2s^2\ 2p^6\ 3s^2\ 3p^6\ 4s^2\ 3d^{10}\ 4p^6\ 5s^2\ 4d^9$	$1s^2\ 2s^2\ 2p^6\ 3s^2\ 3p^6\ 4s^2\ 4g^{16}, 5s^2, 5g^9$
Au(79)	$1s^2\ 2s^2\ 2p^6\ \ldots\ 4f^{14}\ 5d^{10}\ 6s^1$	$6s^2, 5g^{16}, 6h^{23}$

Why the Ulianov Distribution does not require Aufbau, Hund, or Pauli Rules

The Pauling scheme relies on three empirical principles—Aufbau filling order, Hund's rule of maximum multiplicity, and the Pauli exclusion principle—because electrons are treated as point particles with undefined geometry. Thus, additional rules are required to prevent electrons from "falling" into the same state, to explain why certain orbitals fill before others, and to justify the spin patterns observed in atoms.

In the Ulianov framework, none of these auxiliary rules are needed.

- Geometry replaces Aufbau. In UST, the nucleus has a definite geometric structure (the KUPT), and each completed layer dictates the allowed electron-shell geometry. Electrons are extended spherical shells with a mass-pole that must occupy one of the discrete geometric directions permitted by the nuclear structure. Therefore, the order of filling emerges naturally from geometry, not from empirical energy rules.

- Mass-pole orientation replaces Hund's rule. Each electron has a single intrinsic spin orientation determined by its polar mass. Apparent "opposite spins" arise only when two electrons bind face-to-face, with one shell inverted. As a result, Hund's rule is not a separate postulate but a direct consequence of how many geometrically distinct mass-pole directions are available.

- Extended shells eliminate Pauli-style conflicts. Because electrons are not point-like but thin spherical membranes with charge distributed over their surface, the notion of two electrons occupying the same "state" is replaced by whether their mass-poles can or cannot occupy the same geometric location. The Pauli principle becomes a geometric impossibility rather than an imposed constraint: the nucleus provides only one mass-pole direction per slot, so two electrons cannot occupy it simultaneously.

Thus, the Ulianov distribution dispenses with the three most important empirical principles of quantum chemistry. Electron organization is not determined by abstract quantum numbers but by the real three-dimensional geometry of the nucleus and the physical properties of the electron shell itself.

Examples in Metallic Elements

Several transition and noble metals illustrate how the Ulianov Distribution provides a more geometrically grounded interpretation of metallic bonding.

Iron (Fe).

Pauling notation gives

$$1s^2\ 2s^2\ 2p^6\ 3s^2\ 3p^6\ 4s^2\ 3d^6,$$

suggesting only two valence electrons. In UST, the outer nuclear geometry supports a g-layer configuration

$$4g^6$$

with six electrons carrying free, outward-facing mass poles. These six poles naturally align along the Cartesian axes ±x,±y,±z, producing *three-dimensional metallic connectivity* and explaining why iron forms robust crystalline lattices and strong metallic bonds.

Copper (Cu) and Silver (Ag).
Pauling assigns d^9 (Cu) and d^{10}/d^9 (Ag), implying one valence electron. Ulianov distribution recognizes instead a near-complete *g*-shell:

$$4g^9 \text{ (Cu)}, 5g^9 \text{ (Ag)}.$$

Nine available directions correspond to a nearly cubic distribution of poles with one vacancy. This naturally explains:
- excellent electrical conductivity (one mass pole remains weakly bound),
- ease of electron donation,
- stable face-centered cubic (FCC) crystal structures.

Platinum (Pt) and Gold (Au).
For heavier elements, UST includes h-shell configurations. In gold, for example, the highest layer reads

$$6h^{23},$$

where h closes at 32, leaving 23-16=7 mass-poles available even after pairing effects. These seven poles again form a nearly cubic orientation (six directions) plus one spare, providing a natural explanation for:
- gold's remarkable ductility (one loosely constrained pole),
- strong metallic cohesion (six well-anchored poles),
- excellent conductivity (free pole available for conduction).

From "Electron Clouds" to Geometric Shells
The traditional notion of "electron clouds" in metals (a sea of point-like electrons shared by many nuclei) emerges in UST as a macroscopic average of many extended spherical shells (radius ~5 nm for slow electrons). Because shell charge is uniformly spread, the electrostatic repulsion averages out, and only the tiny mass poles interact strongly with the lattice.
This provides a clearer physical picture than the standard "cloud model" and explains:
- why metals form well-ordered crystals,
- why conduction electrons move freely inside the lattice,
- why some materials easily donate or accept electrons,
- why metallic bonds are strong despite apparent electron delocalization.

Thus, the Ulianov Distribution replaces the Pauling scheme with a geometrically grounded, nucleus-driven model that aligns naturally with observed metallic behavior and provides a unified explanation for bonding, conductivity, and crystal formation.

Electron Shell Dynamics in Metals, Insulators, Liquids, and Vacuum in UST
In the Ulianov String Theory (UST), a free electron is not a point-like corpuscle but a *large, thin spherical shell* of negative charge whose radius depends on its velocity. At very low speeds the radius reaches approximately $R_e \approx 5$ nm, while at high velocities relativistic mass increase causes the membrane to shrink to a radius comparable to its de Broglie wavelength. The mass of the electron remains concentrated in a tiny polar region (the "polar mass"), which is the only part capable of producing hard collisions with matter. The shell itself interacts primarily through smooth electrostatic repulsion.

This geometric picture provides a unified explanation for conduction, insulation, electron mobility in liquids and gases, and electron confinement at interfaces. The following subsections summarize the dynamical behavior of the electron membrane in different physical media.

Free Electrons in Crystalline Metals
A metal consists of a highly regular three-dimensional lattice of nuclei surrounded by tightly bound electronic shells. The typical atomic spacing is 1--2 Å, which is approximately 2,000 times smaller than the radius of a low-speed electron shell. Thus, a free electron inside a metal behaves analogously to a highly resilient "soap bubble" moving through a cubic mesh of extremely thin wires.

Because the negative charge on the electron membrane repels the negative outer shells of the atoms symmetrically from all sides, the *net electrostatic force on the shell is nearly zero*. The shell therefore drifts with almost no deformation and very low resistance. The only significant source of scattering comes from rare collisions between the polar mass and the nuclei or other polar masses. Such collisions increase lattice vibration and manifest macroscopically as electrical resistance.

As the electron's drift velocity increases, two effects enhance the scattering rate:
1. the shell shrinks due to the relativistic mass increase, reducing the averaging effect of the membrane and exposing the polar mass more frequently to the lattice;
2. in a given time interval, the electron crosses more lattice cells, increasing the probability of polar-mass collisions.

These two mechanisms provide a natural microscopic basis for the increase in resistivity with temperature and drift speed.

Electron Confinement at Metal–Vacuum or Metal–Air Interfaces
At the boundary of a metal, the electron membrane encounters the negative charge distribution of atmospheric molecules (air), whose electrons approach at thermal velocities (~500 m/s). The spherical shell therefore experiences a dense *dynamic barrier* of negative charges, which repeatedly push it back into the metal.

Although the shell can be penetrated by small particles, the repulsive geometry of the interface acts like a wall of flexible, rapidly moving charges. This explains why electrons do not spontaneously escape metals into air: the escape requires either (i) photoelectric energy, (ii) thermal emission, or (iii) a strong external electric field.

In the UST picture, the electron does not overcome a "quantum barrier" in the traditional sense, instead, it must overcome a real geometric-electrostatic barrier formed by the collision dynamics between the membrane and the rapidly moving charged shells of atmospheric molecules.

Electron Mobility in Liquids and Gases
Liquids retain short-range order but lack long-range crystalline symmetry. In these environments, the electron encounters a constantly shifting landscape of partial charges, molecular dipoles, and dynamic cavities. A large spherical shell, therefore, propagates by repeatedly deforming around the local molecular structure, producing a higher effective resistance compared to that of metals.

In gasses, the electron shell interacts even more strongly with the charged and polarizable surfaces of gas molecules. Because the shell radius greatly exceeds the intermolecular distance, the

interaction resembles that of a large balloon moving through a swarm of charged or polar obstacles. This explains the low mobility of electrons in dense gasses and the strong dependence of the electron drift on the pressure.

Why Amorphous Materials Block Electrons (Insulators)
Amorphous materials, polymers, and glasses lack the geometric regularity of metals. Instead of a uniform cubic mesh, the electron shell encounters a highly irregular pattern of charges, empty spaces, and angular molecular structures. Consequently, the averaging effect that stabilizes the shell in metals is lost. Local imbalances of charge and field gradients pull the membrane in conflicting directions, making penetration energetically unfavorable.

Thus, UST provides a geometric–electrostatic reason why electrons cannot drift freely in insulators: No periodic structure exists to support a stable propagation of the shell. This complements (rather than replaces) the band-gap explanation of solid-state physics, but arises from a more fundamental spatial mechanism.

Electron Pairs and Superconductivity
UST also suggests a microscopic mechanism for the formation of electron pairs in superconductors. When two free electrons approach closely enough for their polar masses to come within a Planck-length distance, the gravitational contact force (enhanced by $1/L_P^2$) becomes enormous and overwhelms the electrostatic repulsion of their shells. The result is a stable "figure-eight" double-shell configuration, which can move inside specially aligned lattice channels without undergoing collisions.

In this configuration:
- the two shells shield each other from lattice interactions,
- the polar masses move inside an effectively "vacuum-like" channel,
- collisions are eliminated,

leading naturally to *zero resistance*, persistent currents, and the Meissner effect.

Unified Picture
Across all environments–metals, gasses, liquids, vacuum, or superconductors—the behavior of electrons in UST emerges from a single invariant structure: **a rotating spherical shell with a polar mass whose size and geometry adapt smoothly to the environment**.

Where standard quantum models describe conduction through statistical wavefunctions, UST provides a direct geometric mechanism that links:
- scattering,
- resistivity,
- conductivity,
- emission phenomena,
- superconductivity.

All of these effects can be explained and understood by the motion, deformation, and interactions of the extended electron spherical shell negative charge rotating membrane and its polar point-like mass, which also provide a better way to understand the wave-particle electron duality.

Ulianov's Formulation of Maxwell's Equations
In conventional electrodynamics, the Maxwell equations are written with the electric current density **J** introduced as a primitive source in the Ampere–Maxwell law. The internal structure of the electron plays no role in the formulation: it is modeled as a point particle, and the magnetic field of a wire is attributed to the flow of point charges.

In the Ulianov String Theory (UST), electrons are not point-like but thin rotating spherical shells containing a distributed negative charge and a localized polar mass. Because all electrons rotate with the same intrinsic spin sense (determined by the polar mass), each shell already carries a microscopic magnetic dipole. In matter, these dipoles normally cancel due to random orientations; however, an applied electric field slightly displaces the shells and biases their spin axes, producing macroscopic polarization **P** and magnetization **M**.

In this microscopic ontology, the current density is not fundamental. Instead, its macroscopic effect is recovered from the time evolution of **P** and **M**:

$$\mathbf{J}\text{calc}=\mathbf{P}\cdot+c\ \nabla\times\mathrm{M}$$

This expression is then inserted into Maxwell's equations, yielding a field-only formulation:

$$\begin{aligned}\nabla\times\mathbf{E}&=-\frac{1}{c}\frac{\partial\mathbf{B}}{\partial t},\\ \nabla\cdot\mathbf{B}&=0,\\ \nabla\cdot\mathbf{D}&=0,\\ \nabla\times\mathbf{H}&=\frac{1}{c}\frac{\partial\mathbf{D}}{\partial t},\end{aligned}$$

with the constitutive definitions

$$\mathbf{D}=\mathbf{E}+4\pi\mathbf{P},\mathbf{H}=\mathrm{B}-4\pi\mathbf{M}$$

Mathematically, this system is strictly equivalent to the standard Maxwell equations, since substituting the definitions of **D** and **H** recovers the usual Ampere–Maxwell law with $\mathbf{J}_{\text{calc}}$:

$$\nabla\times\mathbf{B}=\frac{1}{c}\frac{\partial\mathbf{E}}{\partial t}+\frac{4\pi}{c}\ \mathbf{J}_{\text{calc}}.$$

Physically, this reinterpretation removes the conceptual distinction between magnetism generated by permanent magnets and magnetism generated by electric currents. In UST, both phenomena originate from the same microscopic mechanism: the alignment and displacement of rotating electron shells. A conducting wire does not "create" a magnetic field; it simply aligns a vast preexisting sea of microscopic dipoles associated with the internal motion of electron membranes.

This fields–only formulation of Maxwell's equations provides strong evidence that UST is lifting conceptual veils that still obscure our understanding of the microscopic physics underlying electrons, neutrons, protons, and even photons. When a classical equation contains explicit sums of different contributions, each representing a distinct physical source, and a new theory replaces these sums with a unified underlying mechanism, it strongly suggests that a deeper layer of physical reality is being accessed.

The resulting equations become more elegant, compact, and symmetrically balanced, reflecting the fact that the electromagnetic field emerges from a single geometric principle rather than from separate constructs. In this section, the UST formulation of Maxwell's equations illustrates precisely this unification: what

previously required multiple source terms now follows naturally from membrane dynamics and polarization flows, revealing a more fundamental structure behind classical electrodynamics.

Conclusion

This work presented a unified geometric description of electrons, protons, and atomic structure based on Ulianov String Theory (UST) and showed that a large set of quantities traditionally regarded as fundamental (in particular the masses and radii of the proton and the electron) can be derived from a single microscopic ingredient: the number of imaginary-time steps N_S (the Simoon number) and the fixed Planck-scale geometry of a single Ulianov wormhole. Modern physics has no known mechanism capable of predicting the proton mass, electron mass, or proton and electron radii according to the first principles. Even quantum chromodynamics (QCD), despite its remarkable success in describing quark interactions, ultimately recovers proton mass from numerical lattice calculations involving gluonic energy whose scale is empirically fixed. UST, on the contrary, provides analytic geometric formulas that produce the correct orders of magnitude and surprisingly accurate numerical values from a single microscopic constant.

The internal consistency of the model is striking. Using only the geometric folding of a string composed of N_S Planck-scale spheres, UST reproduces the observed proton radius, the proton mass, the electron mass, and the effective free-electron radius (Re~5 nm). Even simplified versions of the geometry (such as treating the proton as a tightly wound solid sphere and the electron as a thin shell of N_S pearls wrapped into 137 overlapping layers) already generate masses and radii in the correct physical range. This demonstrates that the proton and the electron are not arbitrary point-like objects but the natural outcome of a deeper geometric constraint associated with imaginary-time collapse.

Several novel insights emerge from this picture. First, the fine-structure constant α acquires a clear geometric meaning:

$$N_C = \frac{1}{\alpha}$$

corresponds to the number of layers that overlap in the spherical membrane of the electron. Because the electron shell spreads its charge over N_C layers, its effective charge is $1/N_C$ of the charge of a single UWH_S unit, explaining why the gravitational force F_G between the mass-bearing UWH_T points appears 137 times weaker than the electric force F_E between the charge-bearing UWH_S. The model thus clarifies the long-standing mystery of why electromagnetic interactions dominate over gravity at atomic scales without introducing separate fundamental interactions: gravity and electric forces are identical at the UWH scale, and their apparent imbalance arises from the radically different distributions of mass and charge in the membrane structures.

Second, UST provides a natural mechanism for all bonding phenomena (in nuclei, atomic orbitals, and molecules) based on the simple rule that gravitational contact between mass bearing UWH points T occurs at separations of order L_P, producing an enormous short-range attractive force (SGCF) that mimics the "strong nuclear force" without invoking new interaction types. This allows protons and neutrons to assemble into stable three-dimensional trees (KUPT structures), explains neutron stability inside nuclei and instability outside, can calculate exactly the minimum number of neutrons that are necessary to stabilize a given atomic nucleon, and clarifies why electrons in orbitals always pair with apparent opposite spins: the two shells touch at their mass poles, forcing one to flip upside down. A unified geometric mechanism explains phenomena previously attributed to three separate forces (Coulomb, strong nuclear, and weak nuclear), significantly simplifying the conceptual landscape.

Third, the detailed geometry of the electron shell resolves long-standing paradoxes in condensed-matter physics. A low velocity free electron expands to a radius of several nanometers, moving through a metal like a robust soap bubble navigating a dense wire mesh. Its charge distribution interacts weakly with the atomic lattice, while its tiny mass-point interacts strongly upon collision, producing thermal agitation. As velocity increases, relativistic mass growth shrinks the shell to a radius comparable to the de Broglie wavelength, explaining diffraction and wave–particle duality in a single geometric framework. In superconductors, two electrons can enter direct mass contact and form a stable figure-eight structure sliding through internal vacuum channels, losing all scattering and enabling dissipationless currents. These mechanisms arise naturally from the geometry of the UST membrane, not from abstract probability amplitudes.

Finally, the same geometric electron model leads directly to a new reformulation of Maxwell's equations, in which the current density is not a primitive but an emergent quantity arising from the polarization and magnetization of many rotating shells. In this view, permanent magnets and electromagnets are not fundamentally different: both arise from the coherent alignment of preexisting microscopic magnetic fields carried by each electron. The resulting "fields-only" formulation of Maxwell is mathematically identical to the classical system but conceptually simpler and physically more transparent, revealing that electromagnetism, magnetism, and electron dynamics share a single microscopic origin.

Taken together, these results indicate that UST uncovers a deeper layer of physical reality beneath the Standard Model. Rather than introducing new particles or forces, it reorganizes known physics around a more fundamental geometric principle. This framework is rich in testable predictions (especially in spectroscopy, condensed-matter behavior, electron transport, and transient magnetization) and invites the physics community to examine its implications carefully.

By providing analytic derivations of particle masses, clarifying the structure of electrons and protons, and unifying nuclear, atomic, and electromagnetic phenomena, UST offers a coherent and potentially transformative foundation for modern physics.

References

1. Thomson JJ (1904) On the structure of the atom: an investigation of the stability and periods of oscillation of a number of corpuscles arranged at equal intervals around the circumference of a circle; with application of the results to the theory of atomic structure Philosophical Magazine 7: 237-265.
2. Rutherford E (1911) The scattering of α and β particles by matter and the structure of the atom. Philosophical Magazine 21: 669-688.
3. Rutherford E (1919) Collision of alpha particles with light atoms. iv. an anomalous effect in nitrogen. Philosophical Magazine 37: 581-587.
4. Bohr N (1913) On the constitution of atoms and molecules. Philosophical Magazine 26: 1-25.
5. Heisenberg W (1927) Über den anschaulichen inhalt der

quantentheoretischen kinematik und mechanik. Zeitschrift für Physik 43: 172-198.

6. Schrödinger E (1926) Quantisierung als eigenwertproblem. Annalen der Physik 79: 361–376.
7. Born M (1926) Zur quantenmechanik der stoßvorgänge . Zeitschrift für Physik 37: 863-867.
8. Schrödinger E (1935) Die gegenwärtige situation in der quantenmechanik. Naturwissenschaften 23: 807-812.
9. Ulianov PY (2024) The ulianov bridges: Opening new avenues for the development of modern physics. Available at: https://www.academia.edu/122158212.
10. Ulianov PY (2018) Ulianov string theory: a new representation for fundamental particles . Journal of Modern Physics 2: 77-118.
11. Ulianov PY (2025) The ulianov atomic model. Journal of Chemistry & its Applications 4: 1-11.
12. Ulianov PY (2024) A comprehensive overview of the ulianov theory. International Journal of Media and Networks 2: 01-33.
13. Ulianov PY (2025) Pedras flutuam, folhas afundam: Uma revisã£o da estrutura de massas em fluidos . Physics and Applications International Journal 9: 1-12.
14. Ulianov PY (2025) The true schwarzschild radius: Explaining why matter falls into black holes . Journal of Physical Mathematics & its Applications 3: 1-8.
15. Ulianov PY (2024) Two is better than four! introducing the strong gravitational contact force. Physics & Astronomy International Journal 8: 239-244.
16. Ulianov PY (2024) Comparison of pauling and ulianov electron distribution models. Material Science & Engineering International Journal 8: 49-54.
17. Ulianov PY (2024) Explaining the formation of the 36 smallest known atomic isotopes: From hydrogen to krypton. Material Science & Engineering International Journal 8: 39-47.
18. Ulianov PY (2024) The kepler–ulianov proton tree (kupt): A new model for proton organization, noble gases and nuclear stability. Material Science & Engineering International Journal 8: 39-47.